Entity-based image analysis: A new strategy to map rural settlements from Landsat images

Yan Wang [a,b], Xiaolin Zhu [a,b,c], Tao Wei [d,*], Fei Xu [b], Trecia Kay-Ann Williams [b], Helin Zhang [e]

[a] MNR Key Laboratory for Geo-Environmental Monitoring of Great Bay Area, Shenzhen University, Shenzhen 518060, China
[b] Department of Land Surveying and Geo-Informatics, The Hong Kong Polytechnic University, Hong Kong, China
[c] Otto Poon Charitable Foundation Smart Cities Research Institute, The Hong Kong Polytechnic University, Hong Kong, China
[d] School of Psychology, Shenzhen University, Shenzhen 518060, China
[e] Research Institute of Agriculture and Life Sciences, Seoul National University, Seoul, Republic of Korea

ARTICLE INFO

ABSTRACT

Accurate and timely mapping of rural settlements using medium-resolution satellite imagery, such as Landsat data, is crucial for evaluating rural infrastructure, estimating ecological service values, assessing the quality of life for rural populations, and promoting sustainable rural development. Current mapping techniques, including pixel-based and object-based classifications, primarily focus on identifying artificial surfaces, often failing to capture the complete spatial footprint of rural settlements. These settlements consist of diverse land cover elements, such as houses, roads, agricultural buildings, ponds, parks, and woodlands, which together form entities with distinct local characteristics. To address this limitation, we introduce a novel classification strategy: Entity-Based Image Analysis (EBIA). Inspired by cognitive principles of human visual perception, EBIA groups related land cover elements and differentiates settlements from their background. The key innovation of EBIA lies in its ability to incorporate semantic features within rural settlements, transforming pixel-level land cover classification results (Phase 1) into entity-level settlement mapping results (Phase 2). Our results demonstrate that EBIA effectively maps the comprehensive footprint of rural settlement entities, achieving F1 scores ranging from 0.79 to 0.88 across five globally selected experimental areas. Furthermore, EBIA can be utilized to monitor changes in rural settlements using long-term Landsat imagery. As a new classification strategy, EBIA holds potential for mapping other geographic entities.

1. Introduction

Rural communities constitute a significant portion of the global population, with over 3.4 billion people living in rural settlements as of 2018 (United Nations, 2019). These settlements have undergone notable spatial and temporal changes in recent decades, especially in developing countries such as China and India (Nandi and Mistri, 2022; Tian et al., 2014). While numerous studies have focused on land use and cover change (LUCC) to better understand urban expansion, commonly known as urbanization (Al-Bilbisi, 2019; Bagan and Yamagata, 2012; Goldblatt et al., 2018; Gong et al., 2020; Sarkar Chaudhuri et al., 2017; Xu et al., 2022), the significant changes occurring in rural areas remain largely underexplored on a broad scale (Chen et al., 2017; Nandi and Mistri, 2022). A key challenge is the inadequate accuracy of existing methods for detecting small settlements in rural areas, as suggested by recent studies (Kaim et al., 2022; Wang et al., 2022). Therefore, accurately mapping rural settlements and monitoring their changes is crucial for advancing rural development. This includes studying human mobility (Domon, 2011; Hoffman-Hall et al., 2019), protecting the rural environment (Venter et al., 2016), responding to natural disasters (Chakraborty et al., 2005; Deville et al., 2014), and formulating effective development policies (Barbosa-Brandão et al., 2015).

An effective rural settlement map should accurately capture the complete spatial footprint of rural communities. Rural settlements, as a form of human habitation in rural areas, adhere to the general definition of human settlements. Geographically, a settlement is a community of people residing in a specific location (Tolba and El-Kholy, 1992), encompassing hamlets, villages, towns, and cities. Typically, a settlement includes constructed facilities such as roads, enclosures, field systems, boundary banks and ditches, ponds, parks, woodlands, wind

---

and water mills, manor houses, moats, and churches (Doxiadis, 1970). Unlike urban settlements, rural settlements are characterized by sparser artificial surfaces and a relatively higher proportion of other land cover types essential for supporting rural populations. Connor (2019) defines a rural settlement as a community where multiple families live in close proximity, with fields surrounding the collection of houses and farm buildings. The layout of these settlements can vary, ranging from compact to linear, circular, or grid-like patterns (Connor, 2019). This definition highlights the components, relationships, and configurations of rural settlements. However, the pattern and structure of rural settlements can differ significantly due to varying natural, economic, and cultural conditions, resulting in diverse appearances. For example, in developing countries reliant on agriculture, rural settlements often cover small cropland parcels used for growing vegetables to support self-sufficient communities. In contrast, rural settlements in highly industrialized and developed countries may feature substantial recreational lands (e.g., grasslands, woodlands, ponds) and facilities that support modern lifestyles (e.g., paved parking lots). Regardless of their structure, these settlements can be distinguished from their background in satellite imagery (see examples in Fig. 1).

Mapping the comprehensive footprint of rural settlements is crucial because these areas encompass much more than just rural houses, playing a vital role in various applications. For example, rural settlements reflect the spatial reality related to the lifestyle of the rural population, indicating a distinct structure of rural settlements (Wang, 2016) and highlighting the cultural heritage character (Hartley, 2004; Li et al., 2020). Thus, mapping the comprehensive footprint of settlements can facilitate the exploration of cultural and structural diversity in rural settlements worldwide. In addition, understanding the dynamics of the comprehensive footprint of rural settlements can better support socioeconomic development, such as population redistribution (Kong et al., 2021) and financial support optimization (Barbosa et al., 2022). The comprehensive footprint depicts a boundary for each settlement, offering a large-scale rural settlement inventory, such as the number, size, and shape of settlements. This is invaluable for exploring historical dynamics and spatial distribution of settlements and providing guidance for future rural development and land planning. Furthermore, comprehensive footprint mapping also benefits the evaluation of human-related ecological environments, such as exposure to green spaces (Dennis and James, 2017), and regional carbon cycles and food production influenced by rural population mobility (Wang et al., 2021; Zhang et al., 2022).

Previous studies have explored the use of very high resolution (VHR) satellite images (e.g., submeter) to map rural houses (Li et al., 2022; Pan et al., 2020) and aerial photos to track settlement changes (Liu et al., 2018). With advancements in deep learning and cloud computation

platforms, such as Google Earth Engine (GEE) and Microsoft Planetary Computer, VHR images have been used to produce building footprints globally (Robinson et al., 2022; Sirko et al., 2021). However, the high cost and limited temporal coverage of these VHR satellite imagery pose challenges for long-term mapping and change monitoring. Furthermore, some open geographic databases, such as OpenStreetMap, use volunteers to manually map building footprints, but these building footprints are concentrated in urban areas rather than rural areas (Kaim et al., 2022). Alternatively, medium spatial resolution satellites, such as Landsat, SPOT, and Sentinel-2, are more feasible for rural settlements mapping over large areas and for change monitoring. These medium resolution satellite images have the ability to capture most human-made objects (Hoffman-Hall et al., 2019), such as neighborhoods, shopping centers and open spaces. Landsat stands out for continuous monitoring of settlement change thanks to its distinct advantages, which include a long-term archive spanning over 40 years, good spatial-temporal continuity, abundant spectral information, and consistent sensors and calibration.

The existing studies using medium resolution satellite images to map settlements can be grouped into two classes based on the classification scheme, i.e., general land cover scheme and settlement focused scheme. For the general land cover scheme, several studies generated global land cover and land use products based on Landsat imagery, such as FROM-GLC (Gong et al., 2012), GlobeLand30 (Chen et al., 2015), GLC_FCS30 (Zhang et al., 2021), and CLCD (Yang and Huang, 2021). These products have classification schemes with an artificial surface or built-up class, which can represent settlements in cities and large towns. For the settlement focused scheme, some prominent global human settlement products, such as the Global Human Settlement Layer (GHSL) (European Commission, 2023) and the World Settlement Footprint (WSF) (Marconcini et al., 2021), have been developed by integrating satellite imagery and geospatial vector datasets (e.g., road networks). WSF is a 10 m settlement product based on Sentinel-1 and Sentinel-2 imagery. GHSL contains multiple datasets with various spatial resolutions, such as built-up surfaces (GHS-BUILT-S, 10 m or 100 m), population (GHS-POP, 100 m), and settlement model layers (GHS-SMOD, 1 km). The GHSL datasets are generated by integrating Landsat, Sentinel-2, and global population census. Specifically, GHS-BUILT-S estimates the area of built-up surfaces within each pixel, and GHS-POP then assigns a population number to each pixel based on the population census and GHS-BUILT-S dataset. GHS-SMOD classifies pixels into various settlement typologies, including urban classes (e.g., urban center, urban cluster) and rural classes (e.g., rural cluster, low density grid cell). These typologies are determined based on built-up and population densities, e.g., the "rural cluster" is defined as a cluster of continuous 8-connectivity grid cells with a population of less than 5000. These global settlement products
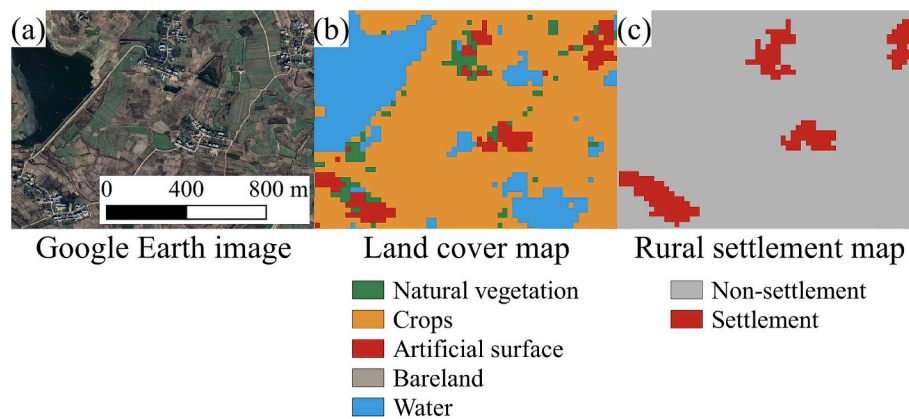
Fig. 1. Examples of rural settlements visualized from high resolution Google Earth images (a); and the corresponding land cover map based on Landsat images (b); and the spatial extent of these settlements which should be mapped from Landsat images (c). These settlements are located around 117.7701 E, 32.3665 N, Anhui Province, China.

have been beneficial for a wide range of environmental and societal research. They have facilitated the estimation of human well-being (McCallum et al., 2022), provided insights into urban growth land subsidence (Cigna and Tapete, 2022), and helped assess population exposure to extreme events (Massaro et al., 2023). In addition to GHSL and WSF products, some studies focused on mapping rural settlements by combining multi-source geospatial datasets, including the combination of road networks and satellite images (Hoffman-Hall et al., 2019), the combination of daytime reflectance and nighttime lights images (Ji et al., 2020), and the combination of passive and active remote sensing images (Xu, 2021).

Existing studies utilizing medium-resolution images often focus on mapping artificial surfaces when analyzing settlements, which are deemed sufficient to represent urban settlement footprints. However, they fail to account for the full range of settlement characteristics in rural areas (Fig. S1 in Appendix A. Supplementary data), where landscapes include a mix of diverse land cover elements, as defined by Connor (2019). This results in a significant underestimation of rural settlement footprints (Kaim et al., 2022; Wang et al., 2022). A settlement footprint is known as a geographic entity comprising different land cover and land use objects, as indicated in Fig. 1(a) (Barbosa et al., 2022; Gong et al., 2023; Johansen and Nielsen, 2012). By ignoring the semantic relationship between different land surface elements within settlements, existing mapping methods can only map large or clustered houses as built-up type or artificial surface type (red pixels in Fig. 1(b)), resulting in a significant underestimation of the actual extent of rural settlements as delineated in Fig. 1(c). Another limitation is the weak representativeness of training samples in the current studies using supervised classification. These studies mainly selected artificial surface samples from urban areas with dense artificial surfaces (Zhang and Roy, 2017; Zhang et al., 2021). However, artificial surfaces (i.e., buildings) in rural settlements are typically mixed with other land covers, such as soils or grass, at the 30 m scale, resulting in weak artificial surface signals in satellite images. The unrepresentative training samples have led to a substantial omission of artificial surfaces in rural areas (Wang et al., 2022). Lastly, geospatial vector datasets, such as road networks and points of interest (POIs) of settlements, could help improve rural settlement mapping, but data availability is not guaranteed or may not be updated timely (Hoffman-Hall et al., 2019), particularly for poor regions that cannot invest in building geospatial databases (Ayanlade et al., 2008; Biljecki et al., 2023).

To solve the above challenges in rural settlement mapping, we proposed a new strategy based on human object recognition, henceforth referred to as the Entity-Based Image Analysis (EBIA) strategy. Human object recognition is a dynamic interplay between bottom-up processing (data-driven analysis of visual information) and top-down processing (semantic/concept-driven interpretation based on prior knowledge) (Gilbert and Sigman, 2007). Unlike the existing pixel- or object-based classification approaches, EBIA considers that different land cover and use types are semantically integrated to form rural settlements (Fig. 1 (c)) which is distinguishable from the background in high and medium resolution images. In this study, EBIA completed rural settlement mapping in a hierarchical way. It consists of two phases: pixel-level land cover classification (Phase 1) and entity-level settlement classification (Phase 2). Phase 1 identifies different land cover elements, and Phase 2 delineates the comprehensive footprint of rural settlements by leveraging the semantic information among different land cover elements. The proposed method was tested in the globally selected rural areas with various structures and compared to existing global settlement products to show its effectiveness.

2. Study area and data

2.1. Study area

Five sites were strategically selected worldwide (Fig. 2(a)) based on three key criteria: (1) the sites should encompass major regions with significant rural populations; (2) they should span various climate zones to represent a diverse range of landscapes; and (3) the settlements should exhibit different patterns (e.g., compact, gridded, or linear) and configurations (e.g., agriculture-based or non-agriculture-based). The chosen rural sites (Fig. 2(b)) include Anhui, China (Site 1), Eure-et-Loir, France (Site 2), Dedza, Malawi (Site 3), Matanzas, Cuba (Site 4), and Jawa Tengah, Indonesia (Site 5). The number of rural settlements in each site varies, ranging from approximately two hundred in Site 2 to nearly two thousand in Site 1. These sites are situated in climate zones classified as Cfa (temperate, no dry season, hot summer), Cfb (temperate, no dry season, warm summer), Cwb (temperate, dry winter, warm summer), Aw (tropical, savannah), and Am (tropical, monsoon), respectively.

Cropland is the dominant land cover type in Sites 1, 2, and 5, indicating extensive agricultural activities, whereas woodland is the primary land cover in Sites 3 and 4. Settlements in Sites 1, 2, and 3 are predominantly compact, while those in Sites 4 and 5 exhibit gridded and linear patterns, respectively. All settlements across the five sites include non-built elements such as trees, vegetable gardens, and bare ground, though these components vary by region. These variations in components are influenced by local natural environments and levels of economic development. The diverse settlement structures across these study sites provide an opportunity to test the applicability of EBIA under different conditions.

Although our study primarily focuses on rural areas, the proposed method is designed to map all settlements present in the given satellite imagery. To further demonstrate the effectiveness of EBIA in mapping settlements across the urban-rural continuum, an additional urban site in Denver, United States, was selected, and its results are reported in the supplementary data (section 7 in Appendix A. Supplementary data).

2.2. Data

2.2.1. Landsat surface reflectance

The input data for mapping rural settlements in this study was Landsat surface reflectance (SR). The Landsat SR dataset (level-2 product) is derived from the original Landsat data after undergoing essential preprocessing steps, including radiometric calibration, geometric correction, and atmospheric correction. This dataset provides more accurate spectral information to compose a time series to delineate land surface objects than the original Landsat data (Masek et al., 2006). For each site, we collected all Landsat surface reference data covering the site from GEE platform. To maximize the availability of cloud-free observations in the target year (e.g., 2020), we collected all Landsat SR data with six months expansion (e.g., July 1st, 2019, to June 30th, 2021 for the target year of 2020) and stacked all data as the time series of the target year.

2.2.2. Auxiliary data

To ensure the feasibility of large-scale settlement mapping, we used the available state-of-the-art land cover product, Dynamic World (Brown et al., 2022), to automatically generate pixel-level land cover sample dataset for the Phase 1 of EBIA (Section 2.2.3). Dynamic World utilizes the Fully Convolutional Neural Network algorithm to produce a land cover data layer with nine categories for each Sentinel-2 tile in near real-time at a spatial resolution of 10 m. The dataset has an overall accuracy of 73.8 % in all classes and a F1 score of 87.5 % in mapping artificial surfaces (Brown et al., 2022). We adopted the classification scheme of Dynamic World, in which orchards were classified as trees. This did not significantly impact our rural settlement mapping results since both orchards and natural trees support the daily life of rural population if they are close to the rural houses. Additionally, we used the high resolution images in Google Earth software to assist the collection of object-level sample dataset and the generation of entity-level full reference data for settlements in the five sites (Section 2.2.3).
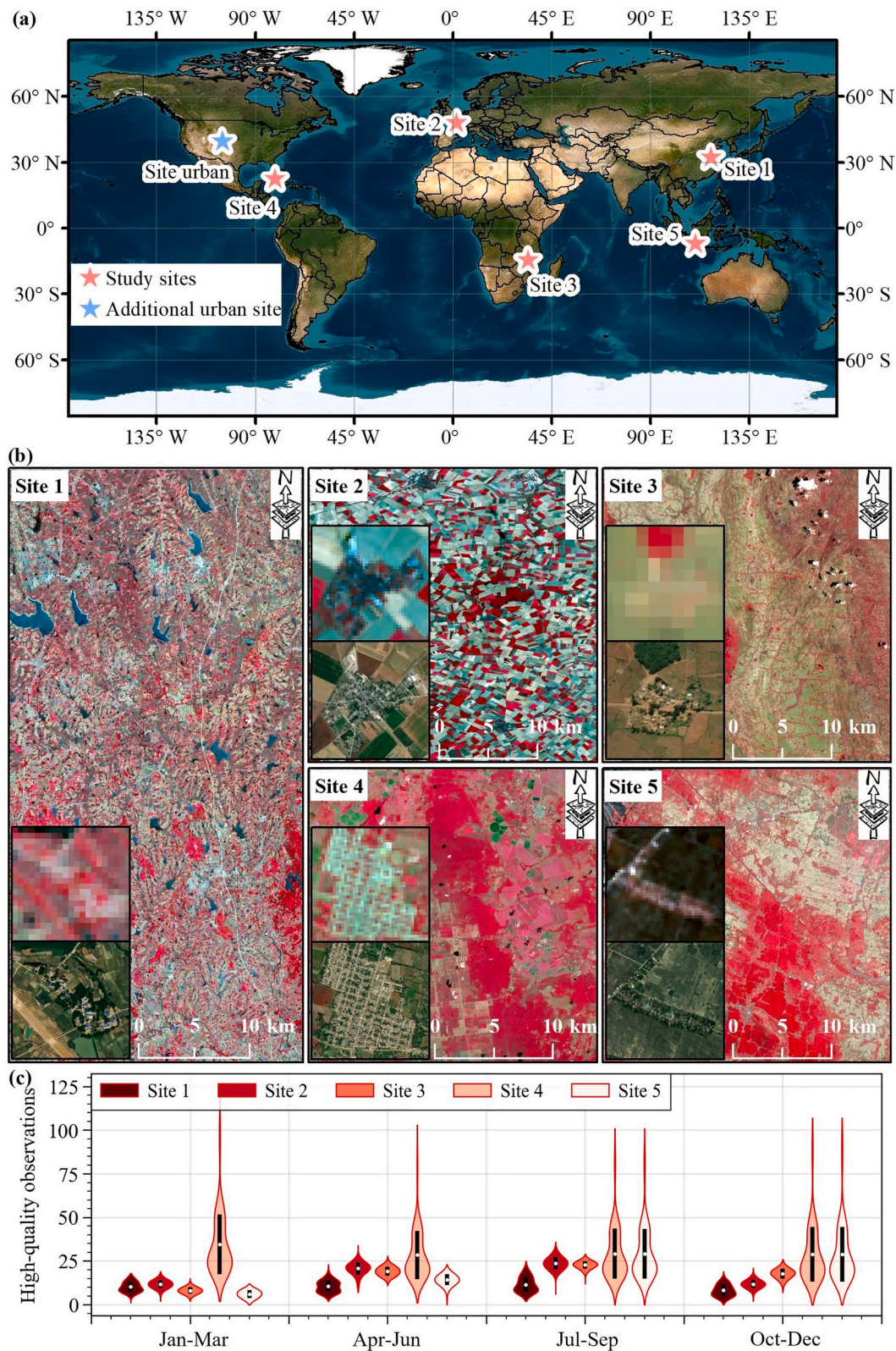
Fig. 2. Locations of study sites and corresponding false-color composition of summer Landsat images acquired in July 2019– June 2021. Five study sites are indicated by red stars and one additional urban site is marked by a blue star on the ESRI base map (a); the false-color composition of Landsat images at China site (Site 1), France site (Site 2), Malawi site (Site 3), Cuba site (Site 4), and Indonesia site (Site 5) are shown in (b); the high resolution Google Earth image (lower left of each site panel) shows an example of rural settlement in each site. The frequency distributions of high-quality Landsat observations within each season at each study site during the two-year period are shown in (c).

We also collected two global human settlement products to quantitatively compare them with the settlement mapping results of our proposed method. These products are the 10 m Global Human Settlement built-up surface dataset (GHS-BUILT-S) in 2018 (European Commission, 2023) and 10 m World Settlement Footprint (WSF) in 2019 (Marconcini et al., 2021). Settlement class in both GHS-BUILT-S and WSF has undergone independent accuracy assessment and got a F1 score of 0.9 and 0.88, respectively (European Commission, 2023; Marconcini et al., 2020). Pixel values of WSF are binary classes (settlement and non-settlement), while pixel values of GHS-BUILT-S depict the distribution of built-up surfaces, expressed in square meters per pixel. Both GHS-BUILT-S and WSF were upscaled from 10 m to 30 m to match the spatial resolution of Landsat. Pixels in the upscaled WSF were marked as settlements if they contained at least one 10-m settlement pixel. Pixels in the upscaled GHS-BUILT-S were marked as settlements if their built-up area is greater than 90 m^2 according to a previous study (Wang et al., 2022).

2.2.3. Sample datasets

We collected sample datasets at pixel-level, object-level, and entity-level for training and validating classifiers, as well as comprehensively testing the accuracy of the mapping results in this study (Table 1). Specifically, we first used an automatic stratified random sampling strategy to collect pixel-level land cover samples based on the Dynamic World dataset for each experimental site. The collection process includes: (1) the original Dynamic World classification results were temporally upscaled to an annual classification result based on the occurrence of class labels; (2) pixels with no land cover change within three consecutive years (the middle year is the target year of mapping) were considered as "sample candidates"; (3) considering the resolution difference between Dynamic World and Landsat data (10 m vs 30 m) and possible georeferencing errors, only sample candidates in relatively homogenous areas, that is, majority pixels in their 9 × 9 pixel window should have same land cover class with themselves, were kept in the sample pool; and (4) in each site, 469 samples for each land cover class (75 % for training and 25 % for testing) were randomly selected from the sample pool. This sample dataset was used for training and validating the random forest classifier for pixel-level land cover classification (Section 3.2.2). It is worth noting that other land cover products besides Dynamic World could be used to collect these pixel-level samples.

Second, we also adopted the stratified random sampling method to generate object-level settlement samples for each experimental site. These object samples were visually interpreted from VHR Google Earth images in the target year (e.g., 2020) and were identified as their settlement type: settlement (stratum 1) or non-settlement (stratum 2). The sample labelling process was guided by three principles based on the definition of rural settlements (Connor, 2019): (1) artificial surface objects are the core of rural settlements. Artificial surface objects that are too small may be salt-and-pepper pixels caused by the mixed pixel issue at the scale of 30 m, thus are beyond our mapping target in this study; (2) besides artificial surfaces, rural settlements also include other land cover objects that support the daily life of the rural population and are close to the artificial surfaces (Porta et al., 2013); and (3) these objects form a settlement cluster which is distinguishable from surrounding background. Finally, we randomly selected 150 samples for each of the

two strata at each experimental site. This sample dataset was used for training and validating the random forest classifier for entity classification (Section 3.2.3).

Last, full reference data of rural settlements in all study sites were generated by trained interpreters based on the definition of rural settlement (Connor, 2019). Specifically, the boundaries of all rural settlements with a detectable size in Landsat data (i.e., 2 × 2 Landsat pixels or larger) were digitized following the common practices used in previous Landsat-based land cover studies (Grinand et al., 2013; Kyzivat and Smith, 2023; Paltan et al., 2015). In addition, the settlement reference in China site was also screened by people who are familiar with the region. These entity-level references were used to assess the accuracy of the settlement mapping results from our proposed method and the compared products (Section 3.2).

3. Methodology

3.1. Entity-based image analysis

A geographic entity is any location or area on the Earth's surface that has identifiable boundaries. These entities can be natural or human-made and are characterized by specific attributes that distinguish them from other areas. A rural settlement is a typical geographic entity. To accurately map the complete spatial footprint of rural settlements (e. g., Fig. 1(c)), an automatic mapping method should meet the following criteria: (1) it can identify the most important land surface component within the geographic entity, such as artificial surfaces in rural settlements; (2) it can use or learn the semantic relationships (e.g., distance, closeness, logic) between different land surface components that organically form the rural settlements; (3) it can delineate the irregular boundaries between the rural settlements and surrounding background, and label diverse pixels within the boundaries as one class, i.e., rural settlement class; and (4) it can incorporate expert knowledge into the mapping process.

Unfortunately, traditional remote sensing image classification strategies (Fig. 3), such as pixel-based, object-based, and scene-based classifications, cannot meet the above criteria. For instance, both pixel- and object-based classifications focus on differentiating land cover and land use classes and label pixels or objects (clusters of similar pixels) based on their own spectral and textural features (Blaschke, 2010; Myint et al., 2011). They treat all land cover and land use classes equally and cannot use the semantic information between land cover and land use objects to identify the boundaries of rural settlements. In recent years, scene classification strategy has been proposed to label each regular image patch (e.g., 256 by 256 pixels) as a class. Classes from scene classification are one level higher than land cover and land use, and the classes can be more semantically meaningful, such as airport, beach, playground, baseball field, etc. Scene classification developed relatively fast due to deep learning technology since deep learning is more capable to learn the abstract information (e.g., object layout and context) from training samples which is needed for labeling a scene as a semantic class (Cheng et al., 2017). However, image scenes with regular patches in scene classification cannot delineate the irregular boundaries of rural settlements.

Here we proposed the entity-based image analysis (EBIA) strategy

Table 1
Summary of sample datasets.

Utilization of samples	Data source	Sample size	Sampling method	labelling method	Sample unit
Train and validation of land cover classification	Dynamic world	3752 pixel-level samples for each site	Stratified random sampling	Automatic labelling	Land cover pixel
Train and validation of settlement classification	High resolution Google Earth images	300 object-level samples for each site	Stratified random sampling	Visual interpretation and expert knowledge	Land cover object
Accuracy assessment of Settlement map	High resolution Google Earth images	All settlements in each site	Full sampling	Visual interpretation and expert knowledge	Settlement entity

	Pixel	**Object**	**Scene**	**Entity**
Mapping target	Image pixel	Cluster of homogeneous pixels	Regular image patch (e.g., 256×256)	Geographic entity
Classification scheme	Land cover and land use	Land cover and land use	Semantic class	Entity class
Input features	Spectrum Texture	Spectrum Texture Statistics	Spectrum Semantic	Spectrum Texture Semantic
Accuracy assessment	Pixel samples Error matrix	Object samples Error matrix Matchiness analysis	Scene samples Error matrix	Entity samples Error matrix Matchiness analysis

Fig. 3. Summary of different remote sensing image classification strategies.

based on cognitive principles of human visual perception to better map rural settlements as geographic entities. Human cognitive principles involve both data-driven bottom-up processing and semantic-driven top-down processing (Gilbert and Sigman, 2007). On the contrary, the traditional classification strategies fairly depend on bottom-up processing. EBIA is different from traditional pixel-, object-, and scene-based classifications in terms of classification scheme, mapping unit, features used, and accuracy validation (Fig. 3). The classification scheme is the target geographic entity (e.g., rural settlements in this study). The mapping unit is irregular image patches that delineate the boundaries of the mapping target. The features used include all levels, from pixel spectral, spatial texture, semantic information, and expert knowledge. Validation was implemented at the entity level by comparing the matchiness between the mapped entities and the ground truth based on the application needs, rather than simply counting pixels correctly classified.

It is worth noting that both object-based classification (also referred to as Geographic Object-Based Image Analysis, GEOBIA) and EBIA label pixel groups instead of individual pixels (Blaschke, 2010; Blaschke et al., 2014), but they have significant differences. First, GEOBIA and EBIA serve distinct purposes and applications. GEOBIA primarily addresses limitations of per-pixel classifications by utilizing information contained in a group of pixels with similar spectral signals. However, mapping diverse entities relevant to human activities, including rural settlements, requires approaches that go beyond GEOBIA methods, as these entities are not delineated by pixels with similar spectral signals. Second, mapping units in GEOBIA are self-defined objects extracted from satellite imagery, such as houses, lakes, and wildfire burn scars. Standard image segmentation with optimized parameters can generally delineate these objects. Conversely, EBIA employs a mapping unit not entirely self-defined from satellite images. Thus, determining the mapping unit for EBIA necessitates a nuanced understanding of human knowledge and is task-dependent. Last, the mapping processes between GEOBIA and EBIA diverge significantly. GEOBIA typically follows a "segmentation-classification" model, where segmentation identifies image objects, and classification labels these objects using information such as tone, size, shape, texture, and topological relationships. In contrast, segmentation is not necessary in EBIA, since the boundary of an entity is delineated by functional features rather than image features. EBIA can employ either an "end-to-end" or hierarchical model to use functional features. With a large volume of entity-level samples, deep learning-based classification

methods can discern the organizational structure of pixels within each meaningful entity in an "end-to-end" fashion. Alternatively, in the hierarchical model, image pixels may initially be labeled as basic, naturally defined elements using per-pixel methods, and then further grouped into meaningful entities based on domain expert knowledge. These differences highlight the potential of EBIA to map such geographic entity.

3.2. Implementation of EBIA in mapping rural settlements

A hierarchical framework which consists of two phases of classification was employed to implement EBIA in mapping rural settlements (Fig. 4). Phase 1 is the pixel-level land cover classification (a bottom-up processing), and Phase 2 is the entity-level settlement classification (a top-down processing). Both phases use a random forest classifier for the classification task (hereafter named Classifier 1 and Classifier 2). Both phases have automatic post-processing which incorporates expert knowledge to eliminate noises and refine results. Post-processing in Phase 1 includes merging land cover types, removing roads, and generating land cover objects, and post-processing in Phase 2 is to refine the classification result. The whole EBIA process is automatic without human-computer interactions. Further details with respect to these procedures are introduced in subsections 3.2.1 to 3.2.3.

3.2.1. Data preprocessing

All available Landsat SR images with a cloud coverage percentage less than 70 % were collected to map settlements in the target year, and pixels contaminated by cloud were masked according to the quality band. Then, two automatic preprocessing steps were conducted. First, the spectral differences caused by sensors (e.g., ETM+ and OLI) were harmonized via a linear transformation method proposed by Roy et al. (2016). Second, four spectral indices were calculated for each image to enhance the discrimination among land covers, including the Enhanced Vegetation Index (EVI) (Liu and Huete, 2019), the Normalized Difference Water Index (NDWI) (McFeeters, 1996), the Normalized Difference Moisture Index (NDMI) (Wilson and Sader, 2002), and the Normalized Burn Ratio (NBR) (García and Caselles, 1991). These four spectral indices and the six spectral bands (blue, red, green, near infrared, and two short-ware infrared) together compose the input data of our method.
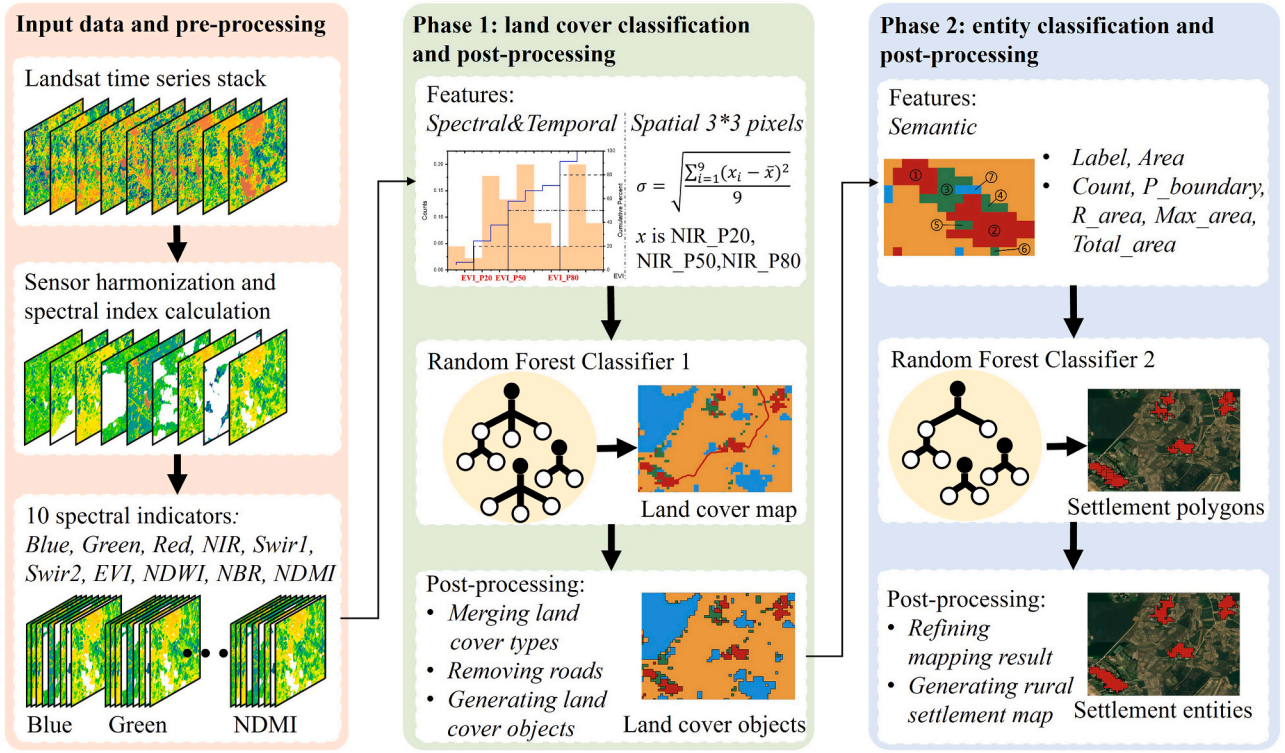
Fig. 4. Flowchart of EBIA for mapping rural settlements.

3.2.2. Pixel-level land cover classification

3.2.2.1. Land cover mapping by random forest classifier.
The pre-processed Landsat images were first classified into general land cover types by a random forest classifier (Classifier 1). The classification scheme of Classifier 1 contained eight land cover types, namely water, tree, grass, flooded vegetation, crops, shrub and scrub, artificial surface, and bareland. Input features include 30 spectral-temporal features and 3 spatial features. Specifically, for each time series of 6 bands and 4 spectral indices, the 20th, 50th, and 80th percentiles at each pixel were extracted as spectral-temporal features. The percentiles represented the amplitude of spectral variation of different land cover classes within the period of the target year, thus providing both spectral and temporal information (Hansen et al., 2011; Zhang and Roy, 2017). The standard deviations of the three percentiles (the 20th, 50th, and 80th) of near-infrared (NIR) time series within a 3×3 pixel window were calculated as the three spatial features, which reflect the local texture. Classifier 1 was trained by 75 % of pixel-level samples (Table 1) and validated by the remaining 25 %. The parameter of the number of decision trees (N_{trees}) in Classifier 1 was set to 200 and other parameters were set to default values based on our experiment results.

3.2.2.2. Post-processing of land cover classification.
Post-processing in Phase 1 had three automatic steps. First, some classes were combined according to their similar functions for supporting the rural population. Specifically, pixels labeled as trees, shrubs, and grass were combined into one class "natural vegetation". Pixels labeled as "flooded vegetation" provide similar functions to water, so these pixels were merged into the class "water". The classification results after combination contained five types, namely "natural vegetation", "crops", "artificial surface", "bareland", and "water".

Second, an automatic approach was designed to remove roads (belonging to the artificial surface class) outside the rural settlements because those roads would affect the subsequent settlement mapping. This approach utilizes the linear pattern of roads in the land cover

classification results (Fig. 5(a) and (b)). Initially, a 5×5 pixel window was created for each artificial surface pixel (Fig. 5(c)). Subsequently, for each artificial surface pixel in the outermost edges of the window, we linked them with the center pixel to form line segments. Then, we calculated the angles between any two adjacent line segments. If the
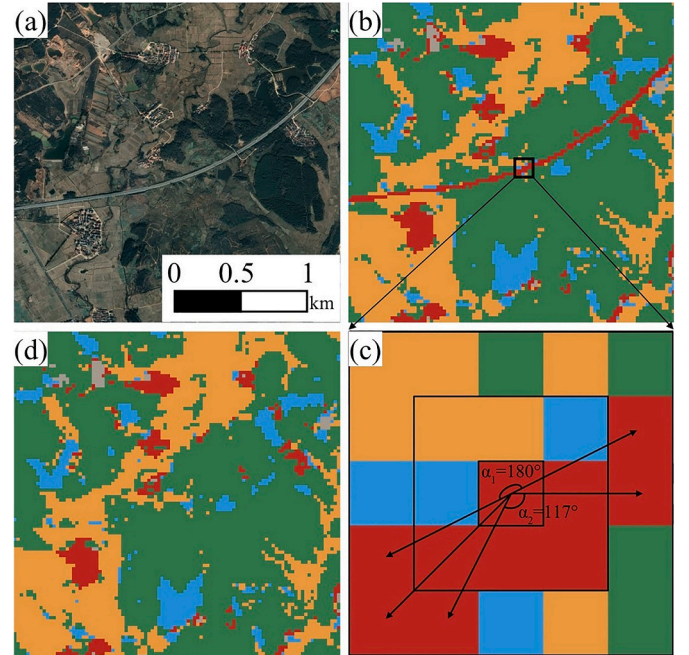

Fig. 5. The approach of removing roads from the land cover classification results. (a) The VHR image showing a road, (b) its corresponding land cover classification result, (c) the schematic diagram of computing the angles of an artificial pixel using a 5×5 pixels window, and (d) the updated classification result after road removal.

center pixel belongs to roads, two of these angles would be obtuse angle (i.e., $>90°$) as the example shown in Fig. 5(c). Therefore, the center pixels with two angles larger than 90° were relabeled as a non-artificial-surface class with the most frequent occurrence in its 3×3 window. After applying this approach to all artificial surface pixels, roads outside the settlements were removed in the classification results (Fig. 5(d)).

Finally, the updated classification results were vectorized to generate different land cover objects. Spatially adjacent pixels with the same land cover type formed an object. These land cover objects were fed into Phase 2 to identify if they belong to a rural settlement entity based on semantic features (see details in Section 3.2.3).

3.2.3. Entity-level settlement classification

3.2.3.1. Settlement mapping by random forest classifier. A new random forest classifier (Classifier 2) was trained for settlement classification using object-level samples (Table 1) and validated by the leave-one-out method. Classifier 2 employed seven semantic features to identify each input land cover object from Phase 1 as either settlement or non-settlement type. These seven semantic features were well designed considering the human knowledge of rural settlements (Table 2). Specifically, for each input object (hereafter referred to as target object, e.g., object 3 in Table 2), the semantic features include two attributes of the target object itself, namely, area (Area, unit: square meter) and land cover label (Label). Label is a binary feature representing whether the land cover type of the target object is artificial surface (1) or not (0). The other five semantic features are based on the topological relationship between the target object and its nearby artificial surface objects (referred to as artificial surface neighbors, e.g., objects 1 and 2 in Table 2). Specifically, these features include the number of artificial surface neighbors (count), the proportion of the length of the target object boundary within a certain distance from the artificial surface neighbors (P_boundary), the relative area of the target object to its artificial surface neighbors (R_area), the maximum area of the artificial surface neighbors (Max_area), and total area of the artificial surface neighbors (Total_area) (see examples in Table 2). To search these artificial surface neighbors for each target object, a distance parameter (i.e., the radius of the searching window) was used. The sensitivity analysis (Fig. S2 in Appendix A. Supplementary data) suggests that a distance parameter of 30 m is appropriate for settlement mapping using Landsat imagery. Therefore, we used 30 m as the parameter to search for

Table 2

Seven semantic features used for the entity-level settlement classification. Feature values were computed for object 3 (i.e., the target object) in the example. Semantic features include attributes of the target object and its topological relationship with two artificial surface neighbors (objects 1 and 2).

Example of land cover objects in a rural settlement

Features	Values	Remark
Label	0	Describe the land cover type of the target object
Area	13,500	Describe the size of the target object (unit: square meter)
Count	2	Describe the number of the artificial surface neighbors
P_boundary	0.375	Describe the proportion of the length of the target object boundary within a certain distance from the artificial surface neighbors
R_area	0.3	Describe the relative area of the target object to its artificial surface neighbors
Max_area	27,000	Describe the maximum area of the artificial surface neighbors (unit: square meter)
Total_area	45,000	Describe the total area of the artificial surface neighbors (unit: square meter)

artificial neighbors in this study.

3.2.3.2. Post-processing of settlement classification. It is worth noting that some small artificial surfaces may exist close to rural settlements. These artificial surfaces are supposed to be part of the nearby rural settlements, but they may be excluded from the settlements by Classifier 2 due to their small areas. To address this, an overlay analysis was done between the artificial surfaces from Classifier 1 and the settlement entity classification results from Classifier 2, enabling us to automatically identify these small artificial surfaces located close to rural settlements but omitted by Classifier 2. These omitted small artificial surfaces were then added back to the nearby settlements.

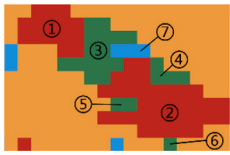### 3.3. Accuracy assessment of settlement classification results

The common sample unit for accuracy assessment can be pixel, block, or polygon (Olofsson et al., 2014). Our purpose is to map the comprehensive footprint of rural settlements rather than artificial surface pixels within those settlements. Therefore, an entity-based accuracy assessment method was used. Specifically, we calculated Intersection over Union (IoU) (Zhou et al., 2019) to quantify the amount of overlap between each settlement in reference data and mapped results. A settlement in the reference data was considered as a correctly detected case (true positive) if its IoU was greater than or equal to the given threshold. Otherwise, the settlement was considered as omitted (false negative). Settlements detected from satellite data but not present in the reference data were considered commission cases (false positive). We selected an IoU threshold of 0.5 to determine if a reference settlement was successfully detected. Error matrices were then constructed. Since the full reference data at five sites only contain settlement objects, non-settlement matchiness (i.e., true negatives) had no value in the error matrices. Three accuracy metrics of mapped settlements, including producer's accuracy, user's accuracy, and F1 score (Hripcsak and Rothschild, 2005) under an IoU of 0.5 (PA^{50}, UA^{50}, and $F1^{50}$) were calculated from the error matrices. Furthermore, we reported the average PA, UA, and F1 score (A-PA, A-UA, and A-F1) across nine IoU thresholds (0.3–0.7 with 0.05 as interval) to get a more comprehensive accuracy assessment. In this way, we assessed the performance of EBIA in the five study sites in 2020.

We compared the mapping results from our method with two existing global settlement datasets to evaluate whether EBIA can offer supplementary information beyond what is currently available in these datasets. Since the GHS-BUILT-S dataset is for 2018 and the WSF dataset is for 2019, we digitized the full reference data of settlements for 2018 and 2019 based on the VHR images. These two datasets were then vectorized to extract settlement polygons for comparison with reference data. GHS-BUILT-S and WSF using 10-m Sentinel-2 as input may detect some smaller settlements that were not delineated in the reference data, so these small settlements were not counted in the accuracy assessment. It is worth noting that the difference of settlement definition between our method and these two products could be the main reason for the accuracy difference. Specifically, we mapped rural settlements based on the definition given by the geography field (Connor, 2019) in which rural settlements include built-up areas and their surrounding lands that are essential for the rural population. On the contrary, both GHS-BUILT-S and WSF datasets only extracted the built-up areas, which would lead to lower IoU values when compared with reference settlement data. The comparison between our method and these two products is unfair but can imply that there is a need to develop a new method for mapping the complete footprint of rural settlements.

To better demonstrate the value of the long-term Landsat archive in rural settlement mapping, we further applied our proposed EBIA method to map the multi-temporal settlement changes in Site 1 (China site) at five-year intervals, spanning from 1990 to 2020. Considering that China has launched a series of rural development policies in the past few

decades, this allows us to evaluate the effectiveness of our method in tracking the dynamics of rural settlements.

4. Results

4.1. Classification results of rural settlements

Fig. 6 illustrates the rural settlement maps in 2020 at five study sites. In Phase 1, Classifier 1 produced 91 % - 92 % overall accuracy for land
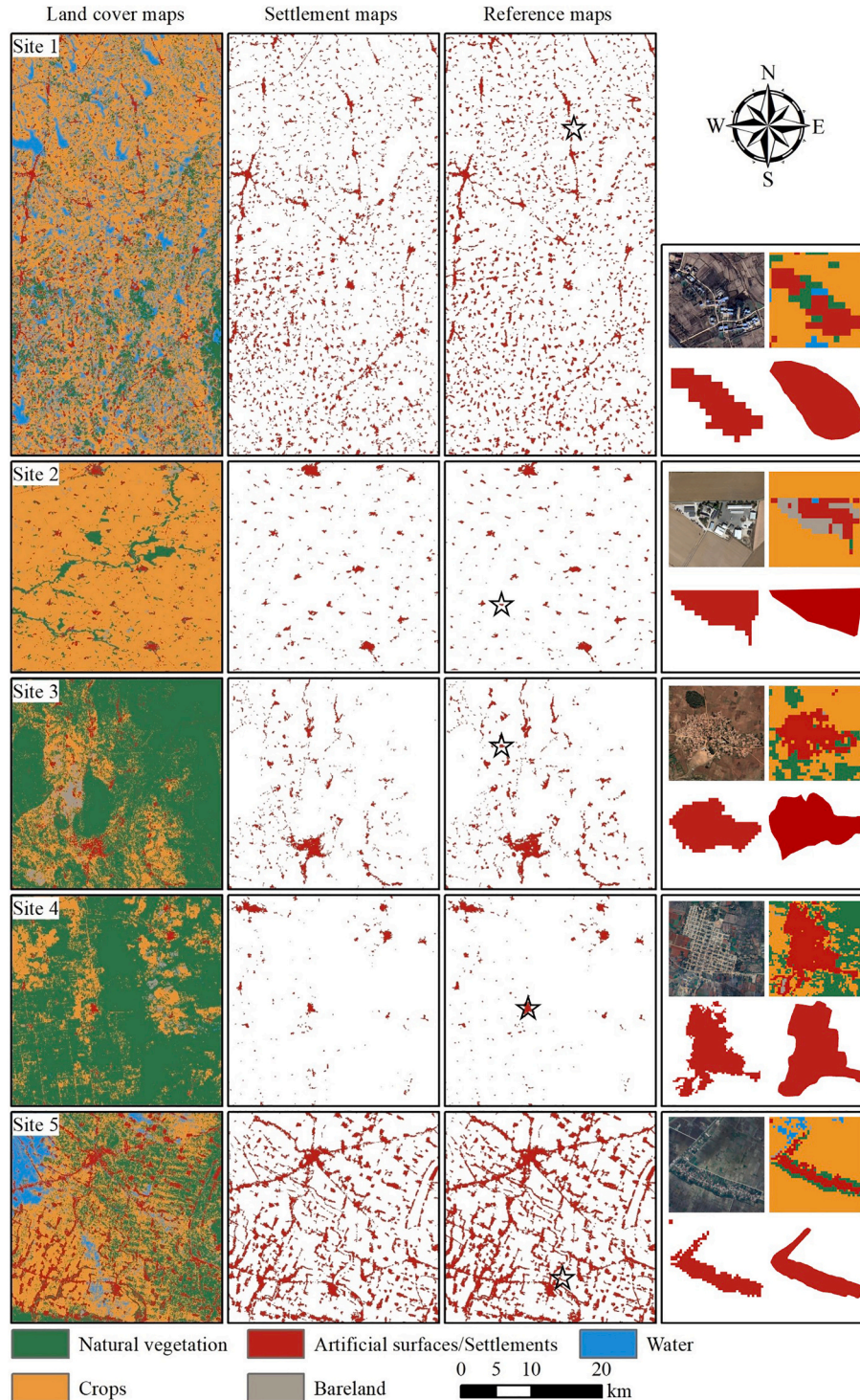
Fig. 6. Classification maps at five study sites: Site 1 in China (top row), Site 2 in France (second row), Site 3 in Malawi (third row), Site 4 in Cuba (fourth row), and Site 5 in Indonesia (bottom row). Each site includes a land cover map from Phase 1 (first column), a settlement map from Phase 2 (second column) and a reference map (third column). Panels in the fourth column show five examples of detected rural settlements in the five sites. These examples are marked with a star in the reference maps. Each panel contains a high resolution Google Earth image (upper left), a land cover map (upper right), a mapped settlement entity (lower left), and a reference settlement entity (lower right). The scale bar pertains to the maps presented in the first three columns.

cover mapping at the five study sites using the validation samples (pixel-level validation samples in Table 1). Classifier 1 successfully mapped most of the artificial surface pixels (first column in Fig. 6). In addition, Classifier 1 detected other land cover types within the spatial extent of rural settlements, although these were highly fragmented. For instance, the zoomed examples (fourth column of Fig. 6) show that there are different land cover elements surrounding these artificial surfaces, including natural vegetation, water bodies, and bare land. In Phase 2, Classifier 2 successfully labeled pixels with different land cover types as rural settlement entities and obtained overall accuracy from 95 % to 97 % in all sites using the leave-one-out validation method (object-level validation samples in Table 1). As a result, the comprehensive footprints in the settlement maps (second column of Fig. 6) showed a high degree of consistency with the reference maps (third column of Fig. 6). EBIA successfully mapped all types of settlements in the additional site of Denver (Fig. S6 in Appendix A. Supplementary data). In urban core areas, EBIA accurately delineated the entire connected residential area as a settlement footprint, while appropriately excluding large urban parks from these footprints. In suburban areas, EBIA identified sparse residential areas as individual settlements, aligning with the settlement definition used in our study. These results in Denver demonstrate the effectiveness of EBIA in mapping settlement footprints across the entire urban-rural continuum.

In 2020, 1798, 222, 464, 187, and 350 settlements in Sites 1–5 were digitized by trained interpreters, respectively, which were used to conduct the quantitative accuracy assessment of our method and the compared products. The accuracy metrics derived from the error matrix (Table S1 in Appendix A. Supplementary data) based on an IoU of 0.5 are very similar to the average values across multiple IoUs (i.e., 0.3–0.7 with a 0.05 interval) (Table 3). Therefore, we used the assessment results at an IoU of 0.5 to compare the performance of different methods. The assessment results indicate that our method accurately mapped the comprehensive footprint of rural settlements at the five sites. The PA^{50} for the five sites ranged from 0.77 at Site 3 to 0.92 at Site 2, while the UA^{50} ranged from 0.76 at Site 2 to 0.94 at Site 5. The $F1^{50}$ for Sites 1–5 were 0.85, 0.83, 0.79, 0.82, and 0.88, respectively, suggesting that the proposed method strikes a good balance between commission errors and omission errors. Site 3 had a relatively low PA^{50} compared to the other sites, possibly due to the difficulty in distinguishing the relatively small buildings from the surrounding background in Landsat imagery. This resulted in more omission errors and thus reduced the PA^{50}.

Our method is also robust in mapping rural settlements of different sizes. We evaluated the performance of EBIA along the urban-rural gradient at Site 1 where a county seat is in the north of the site. The statistics of settlement area along the distance with the county seat show that the rural settlements are generally smaller in areas closer to the large town, which may be caused by the urban syphon effect (Fig. 7). The PA^{50} of our method slightly increases with the settlement area along the urban-rural gradient. EBIA achieved a high F1 score of 0.92 in the additional site of Denver (Table S5 in Appendix A. Supplementary data), indicating its effectiveness in accurately mapping settlement footprints of varying sizes and configurations across the entire urban-rural continuum.

4.2. Comparison with other settlement products

The comparison of results from EBIA with the two global settlement products (GHS-BUILT-S and WSF) demonstrates that EBIA can effectively map the comprehensive footprint of rural settlements, providing valuable supplementary information to these global datasets (Fig. 8 and Table 3). All three methods showed similar spatial patterns when compared with the reference maps, but GHS-BUILT-S and WSF underestimated the footprint of rural settlements at all sites (Fig. 8). EBIA achieved the highest PA^{50}, UA^{50}, and $F1^{50}$ across the five study sites compared to the other two products. WSF had the second highest performance at all sites, with the $F1^{50}$ ranging from 0.60 to 0.77. GHS-BUILT-S achieved a comparable accuracy to WSF. The main reason for the lower accuracy for GHS-BUILT-S and WSF than EBIA is that both attempt to map artificial surfaces within settlements rather than the comprehensive settlement footprint that EBIA maps. Overall, the mean F1 score of GHS-BUILT-S and WSF at the five study sites were 0.60 and 0.66 respectively, which was improved by more than 25 % by our

Table 3

Accuracy assessment of EBIA method and the two compared global settlement products, GHS-BUILT-S and WSF. Metrics with a superscript of 50 indicate that the IoU threshold is set to 0.5. A-PA, A-UA, and A-F1 represent the average metric values across the 9 IoU thresholds (0.3–0.7 with 0.05 as interval). Metrics with the highest values are indicated in bold font.

		EBIA	GHS-BUILT-S	WSF
Site 1	PA^{50}	**0.80**	0.43	0.50
	UA^{50}	0.90	0.83	**0.96**
	$F1^{50}$	**0.85**	0.57	0.66
	A-PA	**0.79**	0.43	0.50
	A-UA	0.90	0.78	**0.94**
	A-F1	**0.84**	0.55	0.65
Site 2	PA^{50}	**0.92**	0.67	0.88
	UA^{50}	**0.76**	0.65	0.53
	$F1^{50}$	**0.83**	0.66	0.66
	A-PA	**0.91**	0.60	0.73
	A-UA	**0.75**	0.57	0.47
	A-F1	**0.82**	0.58	0.57
Site 3	PA^{50}	**0.77**	0.44	0.56
	UA^{50}	0.81	**0.90**	0.65
	$F1^{50}$	**0.79**	0.59	0.60
	A-PA	**0.74**	0.44	0.51
	A-UA	0.80	**0.84**	0.59
	A-F1	**0.77**	0.58	0.55
Site 4	PA^{50}	**0.81**	0.55	0.78
	UA^{50}	**0.83**	0.65	0.77
	$F1^{50}$	**0.82**	0.60	0.77
	A-PA	**0.77**	0.54	0.71
	A-UA	**0.82**	0.62	0.74
	A-F1	**0.79**	0.58	0.72
Site 5	PA^{50}	**0.83**	0.49	0.46
	UA^{50}	0.94	0.69	**0.95**
	$F1^{50}$	**0.88**	0.57	0.62
	A-PA	**0.76**	0.45	0.43
	A-UA	**0.93**	0.58	0.89
	A-F1	**0.84**	0.51	0.58
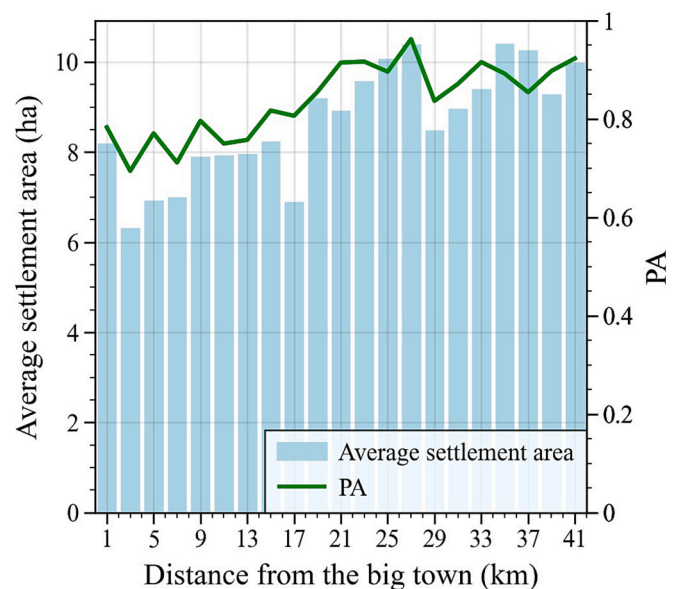
Fig. 7. Average settlement area and producer's accuracy (PA) variation along the urban-rural gradient in Site 1. PA was calculated from the error matrix when an IoU threshold of 0.5 was applied.
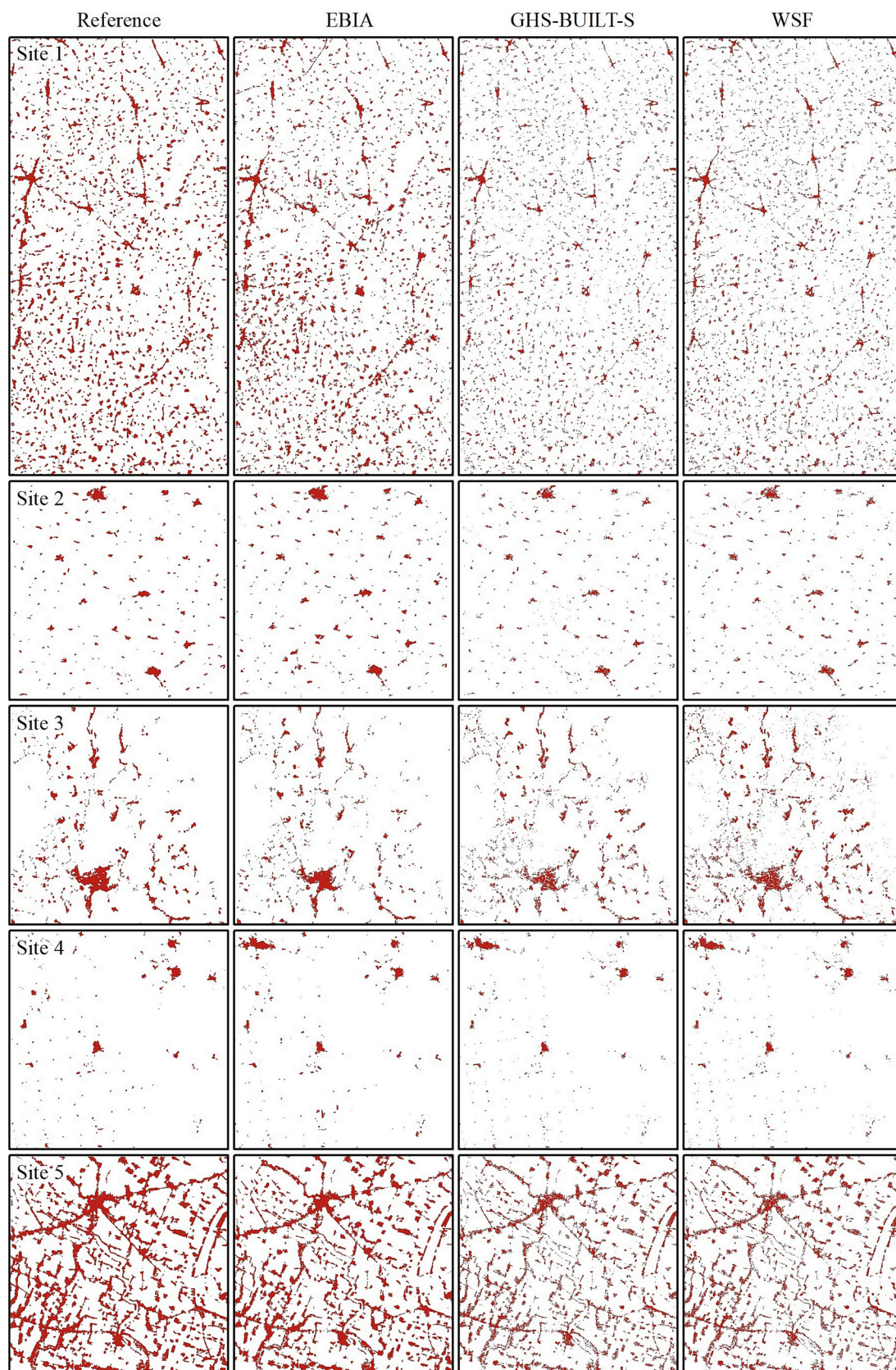
Fig. 8. Reference settlement maps (first column) and settlement mapping results from EBIA (second column), GHS-BUILT-S (third column), and WSF (fourth column) at the five sites (Site 1 in China, Site 2 in France, Site 3 in Malawi, Site 4 in Cuba, and Site 5 in Indonesia).

method. Since the definition of rural settlements in our method differs from that of the two products, this comparison does not indicate which classification method is more accurate. However, it suggests that EBIA is a better choice when the mapping targets are the complete footprint of settlements.

4.3. Multi-temporal mapping for rural settlements

The multi-temporal rural settlement classification results from 1990 to 2020, generated by EBIA, demonstrated a significant linear decrease in both the count and total area of rural settlements in Site 1 (Fig. 9). The linear regression slopes indicate a considerable annual decrease of 2 km^2 for the total area and about 8 for the settlement count. These observed decreases in settlement area and count could be attributed to the rapid socio-economic development in China, which has led to the migration of the rural population to larger cities, such as Hefei, the capital city of Anhui province. This has resulted in a decline in the rural population in the province (data from Statistics Bureau of Anhui Province (ah.gov. cn)). The negative trend in both area and count of rural settlements in Site 1 is consistent with the reported statistics (Fig. 9).

In addition to focusing on economic development in cities, the Chinese government has implemented several strategies to promote rural development, including rural revitalization and land consolidation policies (Tian et al., 2014). These policies have significantly impacted the distribution of rural settlements by merging units and reclassifying rural areas. The evolution of rural settlements in Site1 has been observed in various locations (as shown in the left panel of Fig. 10). Specifically, between 1990 and 2020, 568 settlements disappeared, while 198 emergent settlements were identified in Site 1. Five cases were demonstrated in the multi-temporal false-color Landsat images and evidenced by recent high resolution Google Earth images (as shown in the right panel of Fig. 10). Recent Google Earth images reveal the construction of new settlements in cases 1 and 2 in 2015, while settlements in cases 3–5 have disappeared. Our method successfully captured these changes using long-term Landsat images.

5. Discussion

5.1. Advantages of EBIA strategy

In this study, we proposed the Entity-Based Image Analysis (EBIA) to map rural settlement entities, which were validated at five sites with distinct settlement patterns. Our findings demonstrate that EBIA can
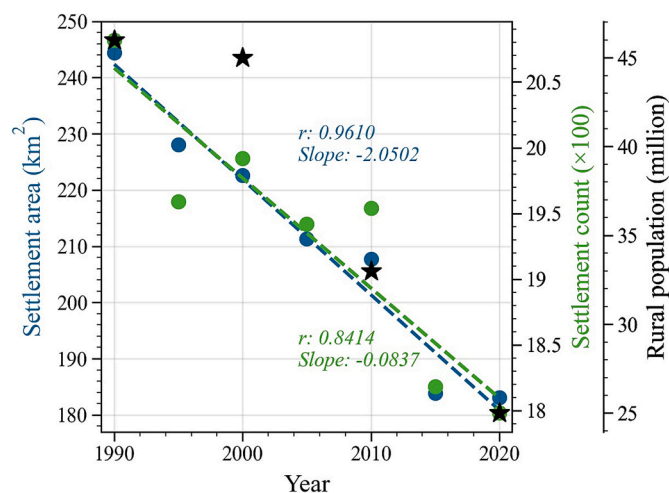

Fig. 9. Changes of total area (blue points) and count (green points) of rural settlements in Site 1 and rural population (black stars) of Anhui province during 1990–2020. (For interpretation of the references to color in this figure legend, the reader is referred to the web version of this article.)

effectively map the comprehensive footprint of rural settlements. The strong performance of EBIA can be attributed to three key strengths.

First, artificial surfaces are the most important element in rural settlement mapping. However, in rural areas, the artificial surface tends to be more fragmented and smaller than other land cover classes. To address this challenge, we designed a sampling framework that automatically selects representative samples for Classifier 1, especially ensuring the representativeness of artificial surface samples in rural settlements. This improved the accuracy of detecting artificial surface pixels in rural areas. Samples were automatically selected from existing land cover products, as in previous studies (Zhang and Roy, 2017; Zhang et al., 2021). However, previous studies selected samples from land cover products with low spatial resolutions (e.g., MCD12Q1), in which samples of artificial surfaces can only represent large cities with dense artificial surfaces. This dilemma prevents classifiers from obtaining high-quality training samples for accurately mapping artificial surfaces in rural areas. Land cover products with spatial resolution at 30 m or higher have been more accessible in recent years (Brown et al., 2022; Chen et al., 2015). These products provide training samples with high representativeness for artificial surfaces at medium scale, which guarantee the classification accuracy in Phase 1.

Second, EBIA mapped rural settlements that contain artificial surfaces, trees, grassland, water bodies and small crop lands, which typically exist within the rural neighborhood to support the lives of the rural population. This mapping approach considers the complete spatial extent of the rural neighborhoods, which has not been addressed by previous studies. Conventional pixel-based methods cannot map the complete footprint of rural settlements, which might not meet the needs of rural studies such as rural eco-environment studies and rural settlement evolution (Li and Song, 2023). GEOBIA identified the built-up objects which cannot cover the complete footprint of rural settlements at the Landsat scale (see examples in Section 4 in Appendix A. Supplementary data). In addition, settlement footprints can be extracted from existing land cover products by merging artificial surfaces and their surrounding land cover elements, which is a simple and efficient approach. For instance, a settlement footprint can be assumed as artificial surfaces plus nearby (e.g., 30 m) cropland if settlements are mainly for agricultural activities (see some examples in Section 8 in Appendix A. Supplementary data). However, for settlements encompassing other components, the land cover elements to be merged need to be predefined, which is subjective and less automated. Supervised classification based on random forest in Phase 2 of EBIA can automatically identify settlement footprints under diverse contexts by employing semantic features among different land cover objects.

Third, expert knowledge was incorporated into the mapping process to address the results that did not follow the definition of geographic entities. In our study, roads outside of rural neighborhoods are not rural settlements, although they were classified as artificial surface in Phase 1. The spatial pattern of roads is linear, making them easily distinguishable from settlements when visualizing land cover maps. Thus, we designed an automatic module to exclude these pixels from the classification results. In addition, the tiny artificial surface objects close to rural settlements omitted by Classifier 2 were added back to settlements in the postprocessing step of phase-2 classification, based on the semantic connections between these tiny artificial surface objects and their nearby settlements. This post-processing step further ensures the completeness of mapped rural settlements.

5.2. The applicability of EBIA to other satellite images

Landsat may provide the coarsest satellite images that can be used to map rural settlements considering the size of rural settlements. Additionally, Landsat offers an important opportunity to analyze historical changes in rural settlements. Therefore, using Landsat for mapping these areas would be very valuable. Our study has demonstrated that using Landsat images to map rural settlements is feasible. However, it is
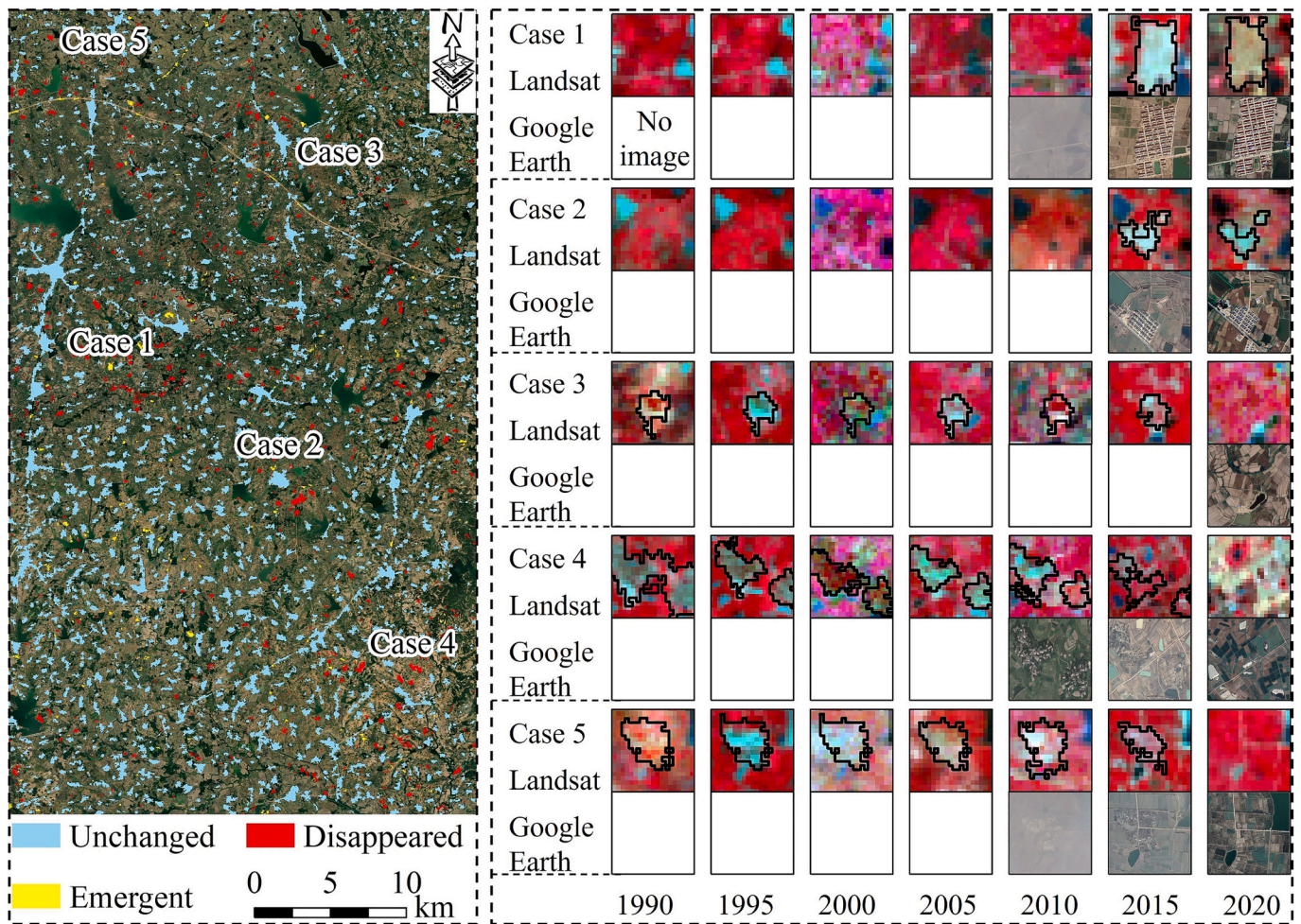
Fig. 10. Dynamics of rural settlements in Site 1 from 1990 to 2020. The left panel shows the spatial distribution of unchanged, disappeared, and emergent settlements in the whole site. The right panel highlights two emergent settlements in 2015 and three disappeared settlements in 2020. Each case in the right panel shows false-color composited Landsat images in the first row and true-color Google Earth images in the second row, spanning from 1990 to 2020 with a five-year interval. White boxes in the second row indicate missing Google Earth images for the specified years. Black polygons on Landsat images represent settlements detected by EBIA.

acknowledged that smaller settlements are more easily detectable by satellite images with spatial resolution higher than Landsat images (Marconcini et al., 2020; Wahbi et al., 2023), and EBIA is also expected to be applicable to these higher resolution satellite images, such as Sentinel-2 and PlanetScope. Thus, we further assessed the applicability of the proposed method for mapping rural settlements using Sentinel-2 and PlanetScope. For sentinel-2, we applied the same filter conditions as those used for Landsat to gather high-quality observations in GEE and used identical spectral bands to those in Landsat images for the classification in Phase 1. PlanetScope has high spatial and temporal resolutions (3 m and 1 day) and provides 8 spectral bands (from coastal blue to NIR) (Planet, 2021). Therefore, given its substantial data volume, we downloaded a maximum of two cloud-free images per month from the European Space Agency website. All the PlanetScope images downloaded (Table S3 in Appendix A. Supplementary data) were used for the classification in Phase 1. We selected a subregion in Site 1 with 10,000 ha area (117.6810 E and 32.2612 N) as the experimental area.

The comparison results across the three satellite images suggested the applicability of EBIA across diverse-scale satellite images (Fig. 11(a)-(d) and Table 4). Quantitatively, compared with results from Landsat, PA^{50}, UA^{50}, and $F1^{50}$ were improved to 0.80, 0.92, and 0.86, respectively, using Sentinel-2, and further improved to 0.83, 0.92, and 0.87, respectively, using PlanetScope in this subregion (Table 4). The grouped bar chart, categorized by different area ranges, further demonstrates the

advantage of higher resolution images in detecting smaller settlements that cannot be detected by Landsat images (Fig. 12). For example, a small settlement missed by Landsat and Sentinel-2 can be detected by PlanetScope (Fig. 11(e)-(h)).

5.3. Implications and limitations

EBIA stands out from traditional pixel- and object-based classification methods as it introduces a novel classification strategy that integrates both bottom-up and top-down processing. Unlike existing settlement products (e.g., GHSL and WSF) that focus on mapping artificial surfaces and buildings, EBIA aims to map the comprehensive footprint of settlements based on local characteristics, thereby offering enhanced support for local and regional studies. Although this study concentrated on mapping settlement footprints in rural areas, EBIA is versatile enough to map footprints for all types of human settlements, provided that the training samples accurately represent settlement structures in both rural and urban regions. This capability makes EBIA a valuable supplement to existing global products. The supplementary experiment conducted in Denver city has demonstrated EBIA's effectiveness in mapping settlements across the entire rural-urban continuum (Section 7 in Appendix A. Supplementary data).

Moreover, EBIA holds significant potential for mapping not only settlements but also other geographic entities, such as wetland parks and

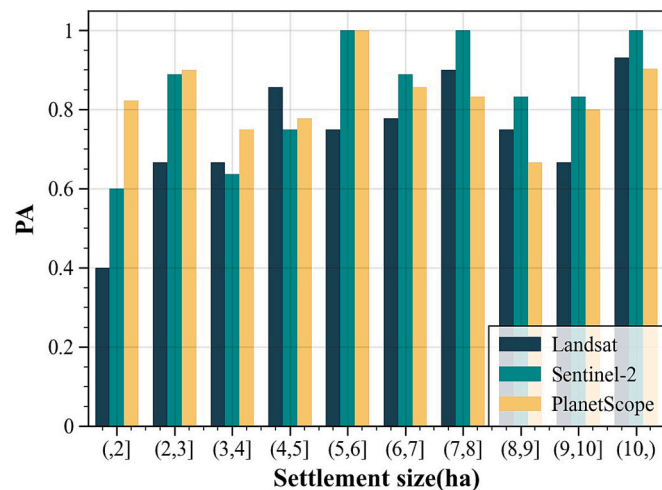| Reference	Landsat	Sentinel-2	PlanetScope
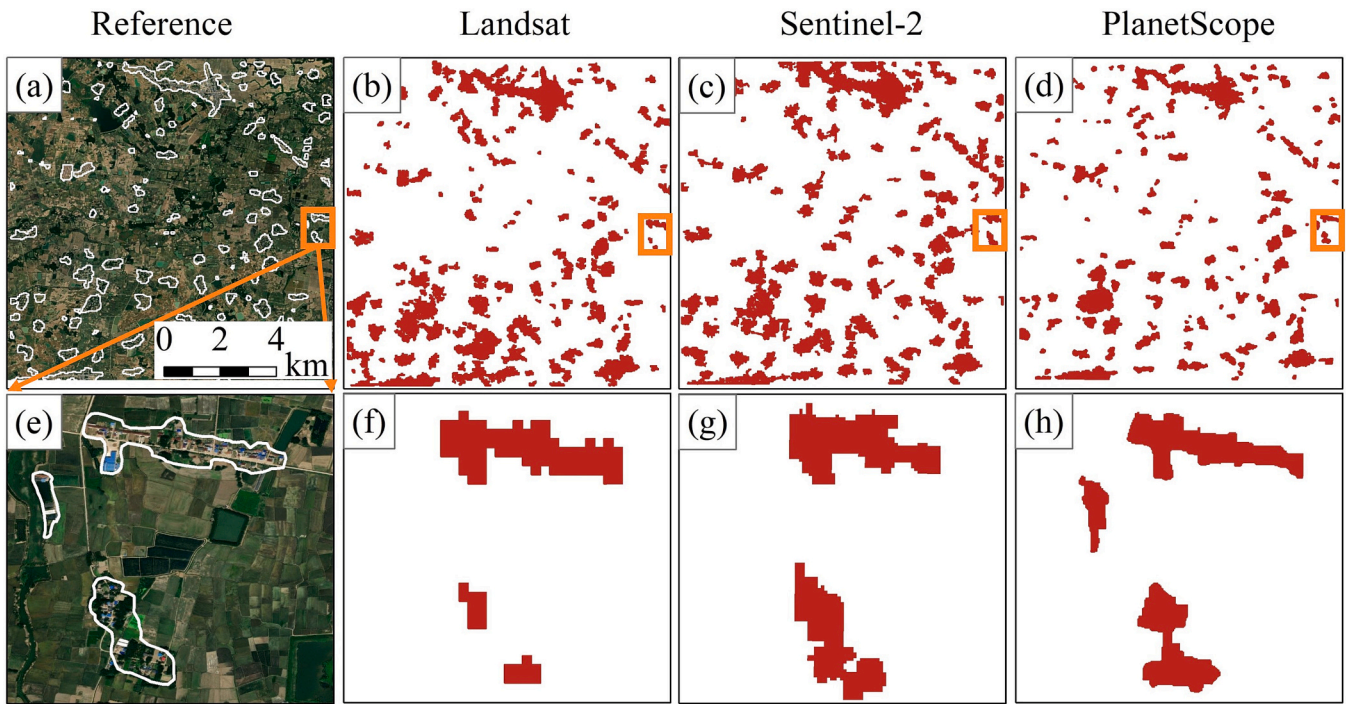
Fig. 11. The reference map (a) in the subregion of Site 1 and classification results using Landsat (b), Sentinel-2 (c), and PlanetScope (d) by EBIA. For the three settlements delineated by the white polygons in (e), the mapping results using Landsat (f), Sentinel-2 (g), and PlanetScope (h) demonstrate the effectiveness of higher resolution satellite images for mapping small rural settlements.

Table 4
Accuracy assessment of EBIA method using three satellite imagery.

Data source	PA^{50}	UA^{50}	F1^{50}
Landsat	0.77	0.88	0.82
Sentinel-2	0.80	0.92	0.86
PlanetScope	0.83	0.92	0.87

Fig. 12. The grouped bar chart showing the variation of PA^{50} with settlement area when mapping rural settlements using Landsat, Sentinel-2, and Planet-Scope imagery.

solar farms (Weise et al., 2020; Plakman et al., 2022). For instance, a wetland park comprises various land cover elements, including water bodies, aquatic plants, and wetland forests (Bwangoy et al., 2010). The spectral signals of these elements differ, leading to varied land cover classifications in pixel- or object-based approaches. EBIA provides a framework for mapping complete wetland parks by exploring the semantic relationships among these land cover elements within the wetland entities.

EBIA has certain limitations when it comes to mapping rural settlements in specific scenarios. First, the spatial resolution of satellite images dictates the smallest size of detectable rural settlements (Kyzivat and Smith, 2023). Due to this limitation, some small settlements were not detected using Landsat images. Higher spatial resolution images can facilitate the detection of smaller settlements (Fig. 12). For region-specific studies, end users can choose appropriate satellite images to capture the footprints of smaller settlements. For instance, in rural Denver, where isolated settlements are quite small (Fig. S5 in Appendix A. Supplementary data), Sentinel-1 and Sentinel-2 imagery with a 10-m resolution were used for land cover classification (Phase 1 of EBIA) to better detect these small rural houses. The assessment results indicate that settlement footprints in rural Denver were accurately mapped (Fig. S7 and Table S5 in Appendix A. Supplementary data).

Second, a large volume of samples is required for the large-scale application of EBIA. The transferability experiment shows generally good performance of EBIA (Table S4 in Appendix A. Supplementary data). The worst performance was observed when the trained model from Site 1 was applied to Site 4, resulting in a 0.05 decrease in the F1 score. For large-scale settlement mapping, local samples are more beneficial for accurately detecting settlement footprints by training locally adaptive classifiers (Woodcock et al., 2001; Zhang and Roy, 2017). However, samples for the classifier in Phase 2 represent the semantic relationships among land cover objects and cannot be automatically extracted from existing land cover products. This poses a challenge for the large-scale application of EBIA. Therefore, further efforts should focus on generating settlement sample pools at a global scale to support large-scale human settlement footprint mapping. This would also advance the development of deep-learning technology for mapping the complete footprint of human settlements.

6. Conclusion

This study proposed a novel classification strategy, Entity-Based Image Analysis (EBIA), to fill the gap in mapping the comprehensive footprint of rural settlements based on Landsat images. We designed EBIA as a hierarchical structure including two phases (i.e., land cover classification at pixel level and settlement classification at entity level). The performance of EBIA was tested at five globally selected study sites. The results have shown that EBIA performed well in mapping rural settlement entities, achieving a mean F1 score of 0.83 for the five sites. Compared with existing products, the major advantage of EBIA is its ability to preserve the comprehensive footprint of the mapped settlements. The strength and flexibility of the EBIA also suggests that it has the potential to map other geographic entities.

CRediT authorship contribution statement

Yan Wang: Writing – review & editing, Writing – original draft, Visualization, Validation, Software, Methodology, Investigation, Formal analysis, Data curation. **Xiaolin Zhu:** Writing – review & editing, Writing – original draft, Supervision, Resources, Project administration, Methodology, Investigation, Funding acquisition, Conceptualization. **Tao Wei:** Writing – review & editing, Writing – original draft, Supervision, Resources, Methodology, Investigation, Funding acquisition, Conceptualization. **Fei Xu:** Writing – review & editing, Writing – original draft, Investigation. **Trecia Kay-Ann Williams:** Writing – review & editing, Investigation. **Helin Zhang:** Writing – review & editing, Investigation.

Declaration of competing interest

This manuscript entitled "Entity-based image analysis: A new strategy to map rural settlements from Landsat images" has not been published and is not under consideration for publication elsewhere. We confirm that there are no known conflicts of interest associated with this manuscript and there has been no significant financial support for this work that could have influenced its outcome.

We have no conflicts of interest to disclose.

Acknowledgments

Appendix A. Supplementary data

Supplementary data to this article can be found online at https://doi.org/10.1016/j.rse.2024.114549.

Data availability

Data will be made available on request.

References

Al-Bilbisi, H., 2019. Spatial monitoring of urban expansion using satellite remote sensing images: a case study of Amman City, Jordan. Sustain. 2019 Vol 11 Page 2260 11, 2260. https://doi.org/10.3390/su11082260.

Ayanlade, A., Orimoogunje, I.O.O., Borisade, P.B., 2008. Geospatial data infrastructure for sustainable development in sub-Saharan countries. Int. J. Digit. Earth 1, 247–258. https://doi.org/10.1080/17538940802149940.

Bagan, H., Yamagata, Y., 2012. Landsat analysis of urban growth: How Tokyo became the world's largest megacity during the last 40 years. Remote Sens. Environ. 127, 210–222. https://doi.org/10.1016/j.rse.2012.09.011.

Barbosa, V., Santé-Riveira, I, Crecente-Maseda, R., Redondo, C.D., Trinidad, J.P., López, J.P., Biempica, R.D., Neto, J.A.F., 2022. A new spatial criteria method to delimit rural settlements towards boundaries equity: land use optimization for decision making in Galicia. NW Spain. Land 11, 800. https://doi.org/10.3390/land11060800.

Barbosa-Brandão, V., Riveira, I.S., Maseda, R.C., 2015. Evolution of legal criteria for the identification and zoning of rural settlements in Galicia, NW Spain. Eur. Plan. Stud. 23, 398–429. https://doi.org/10.1080/09654313.2013.867317.

Biljecki, F., Chow, Y.S., Lee, K., 2023. Quality of crowdsourced geospatial building information: a global assessment of OpenStreetMap attributes. Build. Environ. 237, 110295. https://doi.org/10.1016/j.buildenv.2023.110295.

Blaschke, T., 2010. Object based image analysis for remote sensing. ISPRS J. Photogramm. Remote Sens. 65, 2–16. https://doi.org/10.1016/j.isprsjprs.2009.06.004.

Blaschke, T., Hay, G.J., Kelly, M., Lang, S., Hofmann, P., Addink, E., Feitosa, R.Q., van der Meer, F., van der Werff, H., van Coillie, F., Tiede, D., 2014. Geographic object-based image analysis – Towards a new paradigm. ISPRS J. Photogramm. Remote Sens. 87, 180–191. https://doi.org/10.1016/j.isprsjprs.2013.09.014.

Brown, C.F., Brumby, S.P., Guzder-Williams, B., Birch, T., Hyde, S.B., Mazzariello, J., Czerwinski, W., Pasquarella, V.J., Haertel, R., Ilyushchenko, S., Schwehr, K., Weisse, M., Stolle, F., Hanson, C., Guinan, O., Moore, R., Tait, A.M., 2022. Dynamic World, Near real-time global 10 m land use land cover mapping. Sci. Data 2022 91 9, 1–17. https://doi.org/10.1038/s41597-022-01307-4.

Bwangoy, J.R.B., Hansen, M.C., Roy, D.P., Grandi, G.D., Justice, C.O., 2010. Wetland mapping in the Congo Basin using optical and radar remotely sensed data and derived topographical indices. Remote Sens. Environ. 114, 73–86. https://doi.org/10.1016/j.rse.2009.08.004.

Chakraborty, J., Tobin, G.A., Montz, B.E., 2005. Population evacuation: assessing spatial variability in geophysical risk and social vulnerability to natural hazards. Nat. Hazards Rev. 6, 23–33. https://doi.org/10.1061/(ASCE)1527-6988(2005)6:1(23).

Chen, Jun, Chen, Jin, Liao, A., Cao, X., Chen, L., Chen, X., He, C., Han, G., Peng, S., Lu, M., Zhang, W., Tong, X., Mills, J., 2015. Global land cover mapping at 30m resolution: A POK-based operational approach. ISPRS J. Photogramm. Remote Sens. 103, 7–27. https://doi.org/10.1016/j.isprsjprs.2014.09.002.

Chen, C., Gao, J., Chen, J., 2017. Institutional changes, land use dynamics, and the transition of rural settlements in suburban China: A case study of Huishan District in Wuxi city. Habitat Int. 70, 24–33. https://doi.org/10.1016/j.habitatint.2017.09.011.

Cheng, G., Han, J., Lu, X., 2017. Remote sensing image scene classification: Benchmark and state of the art. Proc. IEEE 105, 1865–1883. https://doi.org/10.1109/JPROC.2017.2675998.

Cigna, F., Tapete, D., 2022. Urban growth and land subsidence: Multi-decadal investigation using human settlement data and satellite InSAR in Morelia. Mexico. Sci. Total Environ. 811, 152211. https://doi.org/10.1016/j.scitotenv.2021.152211.

Connor, G., 2019. Human settlements, in: Dorrell, D., Henderson, J. (Eds.), Introduction to Human Geography. Geological Sciences and Geography Open Textbooks, p. 238.

Dennis, M., James, P., 2017. Evaluating the relative influence on population health of domestic gardens and green space along a rural-urban gradient. Landsc. Urban Plan. 157, 343–351. https://doi.org/10.1016/j.landurbplan.2016.08.009.

Deville, P., Linard, C., Martin, S., Gilbert, M., Stevens, F.R., Gaughan, A.E., Blondel, V.D., Tatem, A.J., 2014. Dynamic population mapping using mobile phone data. Proc. Natl. Acad. Sci. USA 111, 15888–15893. https://doi.org/10.1073/pnas.1408439111.

Domon, G., 2011. Landscape as resource: Consequences, challenges and opportunities for rural development. Landsc. Urban Plan. 100, 338–340. https://doi.org/10.1016/j.landurbplan.2011.02.014.

Doxiadis, C.A., 1970. Man's movement and his settlements? Int. J. Environ. Stud. 1, 19–30. https://doi.org/10.1080/00207237008709391.

European Commission, 2023. GHSL data package 2023. Publ, Off. Eur. Union Luxemb. https://doi.org/10.2760/098587.

García, M.J.L., Caselles, V., 1991. Mapping burns and natural reforestation using thematic mapper data. Geocarto Int. 6, 31–37. https://doi.org/10.1080/10106049109354290.

Gilbert, C.D., Sigman, M., 2007. Brain states: top-down influences in sensory processing. Neuron 54, 677–696. https://doi.org/10.1016/j.neuron.2007.05.019.

Goldblatt, R., Stuhlmacher, M.F., Tellman, B., Clinton, N., Hanson, G., Georgescu, M., Wang, C., Serrano-Candela, F., Khandelwal, A.K., Cheng, W.H., Balling, R.C., 2018. Using Landsat and nighttime lights for supervised pixel-based image classification of urban land cover. Remote Sens. Environ. 205, 253–275. https://doi.org/10.1016/j.rse.2017.11.026.

Gong, P., Wang, J., Yu, L., Zhao, Yongchao, Zhao, Yuanyuan, Liang, L., Niu, Z., Huang, X., Fu, H., Liu, S., Li, C., Li, X., Fu, W., Liu, C., Xu, Y., Wang, X., Cheng, Q., Hu, L., Yao, W., Zhang, Han, Zhu, P., Zhao, Z., Zhang, Haiying, Zheng, Y., Ji, L., Zhang, Y., Chen, H., Yan, A., Guo, J., Yu, Liang, Wang, L., Liu, X., Shi, T., Zhu, M., Chen, Y., Yang, G., Tang, P., Xu, B., Giri, C., Clinton, N., Zhu, Z., Chen, Jin, Jun, Chen, 2012. Finer resolution observation and monitoring of global land cover: first mapping results with Landsat TM and ETM+ data. Int. J. Remote Sens. 34, 2607–2654. https://doi.org/10.1080/01431161.2012.748992.

Gong, P., Li, X., Wang, J., Bai, Y., Chen, B., Hu, T., Liu, X., Xu, B., Yang, J., Zhang, W., Zhou, Y., 2020. Annual maps of global artificial impervious area (GAIA) between 1985 and 2018. Remote Sens. Environ. 236, 111510. https://doi.org/10.1016/j.rse.2019.111510.

Gong, P., Guo, H., Chen, B., Chen, F., He, G., Liang, D., Liu, Z., Sun, Z., Wu, J., Xu, Z., Yan, D., Zhang, H., 2023. iEarth: an interdisciplinary framework in the era of big data and AI for sustainable development. Natl. Sci. Rev. 10. https://doi.org/10.1093/nsr/nwad178.

Grinand, C., Rakotomalala, F., Gond, V., Vaudry, R., Bernoux, M., Vieilledent, G., 2013. Estimating deforestation in tropical humid and dry forests in Madagascar from 2000 to 2010 using multi-date Landsat satellite images and the random forests classifier. Remote Sens. Environ. 139, 68–80. https://doi.org/10.1016/j.rse.2013.07.008.

Hansen, M.C., Egorov, A., Roy, D.P., Potapov, P., Ju, J., Turubanova, S., Kommareddy, I., Loveland, T.R., 2011. Continuous fields of land cover for the conterminous United States using Landsat data: First results from the Web-Enabled Landsat Data (WELD) project. Remote Sens. Lett. 2, 279–288. https://doi.org/10.1080/01431161.2010.519002.

Hartley, D., 2004. Rural Health Disparities, Population Health, and Rural Culture. Am. J. Public Health 94, 1675–1678. https://doi.org/10.2105/AJPH.94.10.1675.

Hoffman-Hall, A., Loboda, T.V., Hall, J.V., Carroll, M.L., Chen, D., 2019. Mapping remote rural settlements at 30 m spatial resolution using geospatial data-fusion. Remote Sens. Environ. 233, 111386. https://doi.org/10.1016/j.rse.2019.111386.

Hripcsak, G., Rothschild, A.S., 2005. Agreement, the F-measure, and reliability in information retrieval. J. Am. Med. Inform. Assoc. 12, 296–298. https://doi.org/10.1197/jamia.M1733.

Ji, H., Li, X., Wei, X., Liu, W., Zhang, L., Wang, L., 2020. Mapping 10-m resolution rural settlements using multi-source remote sensing datasets with the Google Earth Engine platform. Remote Sens. 12, 2832. https://doi.org/10.3390/rs12172832.

Johansen, P.H., Nielsen, N.C., 2012. Bridging between the regional degree and the community approaches to rurality—A suggestion for a definition of rurality for everyday use. Land Use Policy 29, 781–788. https://doi.org/10.1016/j.landusepol.2011.12.003.

Kaim, D., Ziółkowska, E., Grădinaru, S.R., Pazúr, R., 2022. Assessing the suitability of urban-oriented land cover products for mapping rural settlements. Int. J. Geogr. Inf. Sci. 36, 2412–2426. https://doi.org/10.1080/13658816.2022.2075877.

Kong, X., Liu, D., Tian, Y., Liu, Y., 2021. Multi-objective spatial reconstruction of rural settlements considering intervillage social connections. J. Rural. Stud. 84, 254–264. https://doi.org/10.1016/j.jrurstud.2019.02.028.

Kyzivat, E.D., Smith, Laurence C., 2023. Contemporary and historical detection of small lakes using super resolution Landsat imagery: promise and peril. GIScience Remote Sens. 60, 2207288. https://doi.org/10.1080/15481603.2023.2207288.

Li, J., Song, W., 2023. Review of rural settlement research based on bibliometric analysis. Front. Environ. Sci. 10, 1089438. https://doi.org/10.3389/fenvs.2022.1089438.

Li, G., Jiang, C., Du, J., Jia, Y., Bai, J., 2020. Spatial differentiation characteristics of internal ecological land structure in rural settlements and its response to natural and socio-economic conditions in the Central Plains. China. Sci. Total Environ. 709, 135932. https://doi.org/10.1016/j.scitotenv.2019.135932.

Li, X., Xu, W., Huang, Y., Chen, H., Qin, X., Li, Y., Deng, M., Jiang, J., Qin, Y., 2022. Spatial distribution of rural building in China: Remote sensing interpretation and density analysis. Acta Geograph. Sin. 77, 835–851. https://doi.org/10.11821/dlxb202204005.

Liu, H.Q., Huete, A., 2019. A feedback based modification of the NDVI to minimize canopy background and atmospheric noise. IEEE Trans. Geosci. Remote Sens. 33, 457–465. https://doi.org/10.1109/TGRS.1995.8746027.

Liu, D., Toman, E., Fuller, Z., Chen, G., Londo, A., Zhang, X., Zhao, K., 2018. Integration of historical map and aerial imagery to characterize long-term land-use change and landscape dynamics: An object-based analysis via Random Forests. Ecol. Indic. 95, 595–605. https://doi.org/10.1016/j.ecolind.2018.08.004.

Marconcini, M., Metz-Marconcini, A., Üreyen, S., Palacios-Lopez, D., Hanke, W., Bachofer, F., Zeidler, J., Esch, T., Gorelick, N., Kakarla, A., Paganini, M., Strano, E., 2020. Outlining where humans live, the World Settlement Footprint 2015. Sci. Data 7, 242. https://doi.org/10.1038/s41597-020-00580-5.

Marconcini, M., Metz-Marconcini, A., Esch, T., Gorelick, N., 2021. Understanding current trends in global urbanisation - The World Settlement Footprint Suite. GI_Forum 9, 33–38.

Masek, J.G., Vermote, E.F., Saleous, N.E., Wolfe, R., Hall, F.G., Huemmrich, K.F., Gao, F., Kutler, J., Lim, T.K., 2006. A Landsat surface reflectance dataset for North America, 1990-2000. IEEE Geosci. Remote Sens. Lett. 3, 68–72. https://doi.org/10.1109/LGRS.2005.857030.

Massaro, E., Schifanella, R., Piccardo, M., Caporaso, L., Taubenböck, H., Cescatti, A., Duveiller, G., 2023. Spatially-optimized urban greening for reduction of population exposure to land surface temperature extremes. Nat. Commun. 14, 2903. https://doi.org/10.1038/s41467-023-38596-1.

McCallum, I., Kyba, C.C.M., Bayas, J.C.L., Moltchanova, E., Cooper, M., Cuaresma, J.C., Pachauri, S., See, L., Danylo, O., Moorthy, I., Lesiv, M., Baugh, K., Elvidge, C.D., Hofer, M., Fritz, S., 2022. Estimating global economic well-being with unlit settlements. Nat. Commun. 13, 2459. https://doi.org/10.1038/s41467-022-30099-9.

McFeeters, S.K., 1996. The use of the Normalized Difference Water Index (NDWI) in the delineation of open water features. Int. J. Remote Sens. 17, 1425–1432. https://doi.org/10.1080/01431169608948714.

Myint, S.W., Gober, P., Brazel, A., Grossman-Clarke, S., Weng, Q., 2011. Per-pixel vs. object-based classification of urban land cover extraction using high spatial resolution imagery. Remote Sens. Environ. 115, 1145–1161. https://doi.org/10.1016/j.rse.2010.12.017.

Nandi, S., Mistri, T., 2022. Transformation of rural settlement in Salanpur community development block, West Bengal, India. GeoJournal 88, 291–318.

Olofsson, P., Foody, G.M., Herold, M., Stehman, S.V., Woodcock, C.E., Wulder, M.A., 2014. Good practices for estimating area and assessing accuracy of land change. Remote Sens. Environ. 148, 42–57. https://doi.org/10.1016/j.rse.2014.02.015.

Paltan, H., Dash, J., Edwards, M., 2015. A refined mapping of Arctic lakes using Landsat imagery. Int. J. Remote Sens. 36, 5970–5982. https://doi.org/10.1080/01431161.2015.1110263.

Pan, Z., Xu, J., Guo, Y., Hu, Y., Wang, G., 2020. Deep learning segmentation and classification for urban village using a Worldview satellite image based on U-Net. Remote Sens. 12, 1574. https://doi.org/10.3390/rs12101574.

Plakman, V., Rosier, J., van Vliet, J., 2022. Solar park detection from publicly available satellite imagery. GIScience Remote Sens. 59, 462–481. https://doi.org/10.1080/15481603.2022.2036056.

Planet, 2021. Planet satellite imagery and archive [WWW Document]. URL. https://planet.com/products/planet-imagery/ (accessed 12.7.23).

Porta, J., Parapar, J., Doallo, R., Barbosa, V., Santé, I., Crecente, R., Díaz, C., 2013. A population-based iterated greedy algorithm for the delimitation and zoning of rural settlements. Comput. Environ. Urban. Syst. 39, 12–26. https://doi.org/10.1016/j.compenvurbsys.2013.01.006.

Robinson, C., Ortiz, A., Park, H., Lozano, N., Kaw, J.K., Sederholm, T., Dodhia, R., Ferres, J.M.L., 2022. Fast building segmentation from satellite imagery and few local labels. Presented at the Proceedings of the IEEE/CVF Conference on Computer Vision and Pattern Recognition 1463–1471.

Roy, D.P., Kovalskyy, V., Zhang, H.K., Vermote, E.F., Yan, L., Kumar, S.S., Egorov, A., 2016. Characterization of Landsat-7 to Landsat-8 reflective wavelength and normalized difference vegetation index continuity. Remote Sens. Environ. 185, 57–70. https://doi.org/10.1016/j.rse.2015.12.024.

Sarkar Chaudhuri, A., Singh, P., Rai, S.C., 2017. Assessment of impervious surface growth in urban environment through remote sensing estimates. Environ. Earth Sci. 76, 541. https://doi.org/10.1007/s12665-017-6877-1.

Sirko, W., Kashubin, S., Ritter, M., Annkah, A., Bouchareb, Y.S.E., Dauphin, Y., Keysers, D., Neumann, M., Cisse, M., Quinn, J., 2021. Continental-scale building detection from high resolution satellite imagery. https://doi.org/10.48550/arXiv.2107.12283.

Tian, G., Qiao, Z., Gao, X., 2014. Rural settlement land dynamic modes and policy implications in Beijing metropolitan region. China. Habitat Int. 44, 237–246. https://doi.org/10.1016/j.habitatint.2014.06.010.

Tolba, M.K., El-Kholy, O.A., 1992. Human settlements. In: Tolba, M.K., El-Kholy, O.A. (Eds.), The World Environment 1972–1992: Two Decades of Challenge. Springer, Netherlands, Dordrecht, pp. 505–527. https://doi.org/10.1007/978-94-011-2280-1_17.

United Nations, 2019. World Urbanization Prospects: The 2018 Revision (ST/ESA/SER.A/420). Department of Economic and Social Affairs, Population Division. United Nations, New York.

Venter, O., Sanderson, E.W., Magrach, A., Allan, J.R., Beher, J., Jones, K.R., Possingham, H.P., Laurance, W.F., Wood, P., Fekete, B.M., Levy, M.A., Watson, J.E. M., 2016. Sixteen years of change in the global terrestrial human footprint and implications for biodiversity conservation. Nat. Commun. 71 (7), 1–11. https://doi.org/10.1038/ncomms12558.

Wahbi, M., Bakali, I.E., Ez-zahouani, B., Azmi, R., Moujahid, A., Zouiten, M., Alaoui, O. Y., Boulaassal, H., Maatouk, M., Kharki, O.E., 2023. A deep learning classification approach using high spatial satellite images for detection of built-up areas in rural zones: case study of Souss-Massa region - Morocco. Remote Sens. Appl. Soc. Environ. 29, 100898. https://doi.org/10.1016/j.rsase.2022.100898.

Wang, Y., 2016. A Sustainable Approach for Post-Disaster Rehabitation of Rural Heritage Settlements. Sustain. Dev. 24, 319–329. https://doi.org/10.1002/sd.1632.

Wang, S., Bai, X., Zhang, X., Reis, S., Chen, D., Xu, J., Gu, B., 2021. Urbanization can benefit agricultural production with large-scale farming in China. Nat. Food 2, 183–191. https://doi.org/10.1038/s43016-021-00228-6.

Wang, N., Zhang, X., Yao, S., Wu, J., Xia, H., 2022. How good are global layers for mapping rural settlements? Evidence from China. Land 11, 1308. https://doi.org/10.3390/land11081308.

Weise, K., Höfer, R., Franke, J., Guelmami, A., Simonson, W., Muro, J., O'Connor, B., Strauch, A., Flink, S., Eberle, J., Mino, E., Thulin, S., Philipson, P., van Valkengoed, E., Truckenbrodt, J., Zander, F., Sánchez, A., Schröder, C., Thonfeld, F., Fitoka, E., Scott, E., Ling, M., Schwarz, M., Kunz, I., Thürmer, G., Plasmeijer, A., Hilarides, L., 2020. Wetland extent tools for SDG 6.6.1 reporting from the Satellite-based Wetland Observation Service (SWOS). Remote Sens. Environ. 247, 111892. https://doi.org/10.1016/j.rse.2020.111892.

Wilson, E.H., Sader, S.A., 2002. Detection of forest harvest type using multiple dates of Landsat TM imagery. Remote Sens. Environ. 80, 385–396. https://doi.org/10.1016/S0034-4257(01)00318-2.

Woodcock, C.E., Macomber, S.A., Pax-Lenney, M., Cohen, W.B., 2001. Monitoring large areas for forest change using Landsat: Generalization across space, time and Landsat sensors. Remote Sens. Environ., Landsat 7 78, 194–203. https://doi.org/10.1016/S0034-4257(01)00259-0.

Xu, R., 2021. Mapping rural settlements from Landsat and Sentinel time series by integrating pixel- and object-based methods. Land 10, 244. https://doi.org/10.3390/land10030244.

Xu, F., Heremans, S., Somers, B., 2022. Urban land cover mapping with Sentinel-2: a spectro-spatio-temporal analysis. Urban Inform. 1, 8. https://doi.org/10.1007/s44212-022-00008-y.

Yang, J., Huang, X., 2021. The 30 m annual land cover dataset and its dynamics in China from 1990 to 2019. Earth Syst. Sci. Data 13, 3907–3925. https://doi.org/10.5194/essd-13-3907-2021.

Zhang, H.K., Roy, D.P., 2017. Using the 500 m MODIS land cover product to derive a consistent continental scale 30 m Landsat land cover classification. Remote Sens. Environ. 197, 15–34. https://doi.org/10.1016/j.rse.2017.05.024.

Zhang, X., Liu, L., Chen, X., Gao, Y., Xie, S., Mi, J., 2021. GLC_FCS30: global land-cover product with fine classification system at 30 m using time-series Landsat imagery. Earth Syst. Sci. Data 13, 2753–2776. https://doi.org/10.5194/essd-13-2753-2021.

Zhang, X., Brandt, M., Tong, X., Ciais, P., Yue, Y., Xiao, X., Zhang, W., Wang, K., Fensholt, R., 2022. A large but transient carbon sink from urbanization and rural depopulation in China. Nat. Sustain. 5, 321–328. https://doi.org/10.1038/s41893-021-00843-y.

Zhou, D., Fang, J., Song, X., Guan, C., Yin, J., Dai, Y., Yang, R., 2019. IoU loss for 2D/3D object detection, in: 2019 International Conference on 3D Vision (3DV). In: Presented at the 2019 International Conference on 3D Vision (3DV), pp. 85–94. https://doi.org/10.1109/3DV.2019.00019.